Geol. Mag. **144** (*1*), *2007, pp. 1–19. © 2006 Cambridge University Press*

doi:10.1017/S0016756806002937 First published online 21 December 2006 *Printed in the United Kingdom*

The Mamonia Complex (SW Cyprus) revisited: remnant of Late Triassic intra-oceanic volcanism along the Tethyan southwestern passive margin

H. LAPIERRE*, D. BOSCH‡, A. NARROS*, G. H. MASCLE*§, M. TARDY ¶ & A. DEMANT‖

*Laboratoire Géodynamique des Chaînes Alpines, UMR-CNRS 5025, Université J. Fourier, Maison des Géosciences, B. P. 53, F. 38041 Grenoble Cedex, France

‡Laboratoire de Tectonophysique, UMR-CNRS 5568, Institut des Sciences de la Terre, de l'Eau et de l'Espace de Montpellier, CC049, Université de Montpellier II, Place Eugène Bataillon, F. 34095 Montpellier Cedex 05, France

¶Laboratoire Géodynamique des Chaînes Alpines, UMR-CNRS 5025, Université de Savoie, F. 73376 Le Bourget du Lac, France

‖Laboratoire de Pétrologie magmatique, Université Paul Cézanne (Aix-Marseille), case courrier 441, F. 13397 Marseille Cedex 20, France

(*Received* 21 June 2005; *accepted* 11 May 2006)

Abstract – Upper Triassic volcanic and sedimentary rocks of the Mamonia Complex in southwestern Cyprus are exposed in erosional windows through the post-Cretaceous cover, where the Mamonia Complex is tectonically imbricated with the Troodos and Akamas ophiolitic suites. Most of these Upper Triassic volcanic rocks have been considered to represent remnants of Triassic oceanic crust and its associated seamounts. New Nd and Pb isotopic data show that the whole Mamonia volcanic suite exhibits features of oceanic island basalts (OIB). Four rock types have been distinguished on the basis of the petrology and chemistry of the rocks. Volcanism began with the eruption of depleted olivine tholeiites (Type 1) and oceanic island tholeiites (Type 2) associated with deep basin siliceous and/or calcareous sediments. The tholeiites were followed by highly phyric alkali basalts (Type 3) interbedded with pelagic Halobia-bearing limestones or white reefal limestones. Strongly LREE-enriched trachytes (Type 4) were emplaced during the final stage of volcanic activity. Nd and Pb isotopic ratios suggest that tholeiites and mildly alkali basalts derived from partial melting of heterogeneous enriched mantle sources. Fractional crystallization alone cannot account for the derivation of trachytes from alkaline basalts. The trachytes could have been derived from the partial melting at depth of mafic material which shares with the alkali basalts similar trace element and isotopic compositions. This is corroborated by the rather similar isotopic compositions of the alkali basalts and trachytes. The correlations observed between incompatible elements (Nb, Th) and εNd and Pb isotopic initial ratios suggest that the Mamonia suite was derived from the mixing of a depleted mantle (DMM) and an enriched component of High μ ($\mu = {}^{238}U/{}^{204}Pb$, HIMU) type. Models using both Nd and Pb isotopic initial ratios suggest that the depleted tholeiites (Type 1) derived from a DMM source contaminated by an Enriched Mantle Type 2 component (EM2), and that the oceanic tholeiites (Type 2), alkali basalts (Type 3) and trachytes (Type 4) were derived from the mixing of the enriched mantle source of the depleted tholeiites with a HIMU component. None of the Mamonia volcanic rocks show evidence of crustal contamination. The Upper Triassic within-plate volcanism likely erupted in a small southerly Neotethyan basin, located north of the Eratosthenes seamount and likely floored by oceanic crust.

Keywords: Late Triassic volcanism, SW Cyprus, Pb–Nd, oceanic island basalts, Neotethys opening.

1. Introduction

The Neotethyan ophiolitic suites which extend from the eastern Mediterranean (Antalya, Troodos, Hatay, Baër-Bassit) up to the Persian Gulf (Samail nappes in Oman: Béchennec *et al.* 1989, 1991) and the Himalayas (Spontang ophiolites: Bassoullet *et al.* 1980*a*,*b*; Colchen, Mascle & Van Haver, 1986; Cannat & Mascle, 1990; Corfield, Searle & Green, 1999; Mahéo *et al.* 2000) are often tectonically associated with Permian and Upper Triassic volcanic rocks stratigraphically connected with pelagic and/or reefal limestones. In the eastern Mediterranean area (Antalya and Hatay in southern Turkey, Mamonia Complex from Cyprus; Fig. 1), this volcanism is dated as Late Triassic (Marcoux, 1970; Dumont *et al.* 1972; Robertson & Waldron, 1990) on the basis of pelagic bivalves (Halobia), ammonites, corals and microfaunas. In the Baër-Bassit region (NW Syria), two volcanic episodes are recorded, a well-known and widespread Late Triassic event and an Early to Middle Jurassic (Pliensbachian–Bajocian: Al-Riyami *et al.* 2000) event, considered previously as Late Jurassic to Early Cretaceous (Lapierre & Parrot, 1972; Parrot, 1974*a*,*b*;

§Author for correspondence: Georges.Mascle@ujf-grenoble.fr

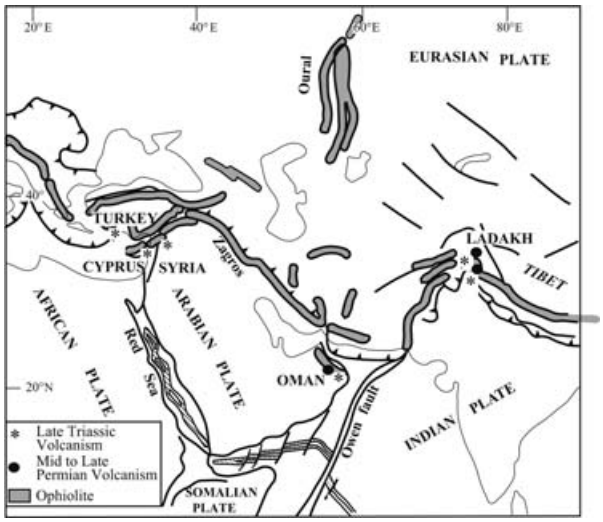

Figure 1. Sketch map of the Neotethyan ophiolites and the Permo-Triassic volcanic sequences (after Searle, 1983).

Delaune-Mayère & Parrot, 1976; Rocci *et al.* 1980; Delaune-Mayère, 1984). The association of Late Triassic submarine volcanic rocks with reefal and platform carbonates and/or deep-water carbonates and radiolarites is systematically observed in the entire Neotethyan ophiolitic belt (Fig. 1) and sets the problem of the geodynamic setting of the Late Triassic magmatism.

We started a new petrochemical study of the Mamonia volcanic rocks using both trace element and isotopic chemistry (Nd, Sr and Pb), in order to check the occurrence of a preserved Late Triassic oceanic crust in Cyprus as proposed by Malpas, Calon & Squires (1993). In this paper, we show that the Late Triassic volcanic rocks of the Mamonia Complex represent the remnants of intra-oceanic island volcanoes which range from LREE-depleted tholeiitic olivine basalts to trachytes through oceanic island tholeiites and clinopyroxene–plagioclase-rich alkali basalts. On the basis of these data, we propose a reconstruction of the Mamonia geodynamic setting during Late Triassic times and a model accounting for the tectonic imbrication of the Mamonia and Troodos ophiolitic complexes in Cyprus.

2. Geological features of the Troodos and Mamonia complexes

The Campanian to Maastrichtian Troodos ophiolitic complex represents the basement of the island of Cyprus, where it is widely exposed (Gass, 1980). It has experienced extensive Late Tertiary uplift of some 2000 m centred on a serpentinite diapir beneath the Troodos summit. From base to top the Troodos ophiolitic suite comprises the very classical ophiolite succession: (1) foliated harzburgite, (2) cumulate plutonic rocks, (3) isotropic gabbros and plagiogranites, (4) sheeted dyke complex and (5) basaltic flows (Gass, 1980). The uppermost basaltic flows are associated and overlain by iron- and manganese-rich sediments (umbers) and radiolarian cherts of Late Cretaceous age (Perapedhi Formation).

Along the northern Troodos margin, these formations are unconformably overlain by the Late Cretaceous to Tertiary sedimentary cover. Along the south and southwestern Troodos margins, the Perapedhi sediments grade upwards into the tuffaceous sandstones and benthonitic clays of the Kannaviou Formation (Lapierre, 1968; Ealey & Knox, 1975; Robertson, 1977) which becomes tectonically overlain by a structural complex made of serpentinized harzburgite on which rest the Late Triassic to Late Cretaceous volcanic rocks and sediments of the Mamonia Complex. Tectonic slices of metamorphic rocks (Ayia Varvara Formation: Malpas, Calon & Squires, 1993) and Troodos ophiolitic rocks are imbricated within the Mamonia tectonic pile (Ayia Varvara section, Fig. 2). A Late Cretaceous to Quaternary sedimentary sequence unconformably covers the Troodos ophiolite and the Mamonia Complex.

The igneous and sedimentary rocks of the Mamonia Complex are subdivided into two main tectonostratigraphic units: the Petra tou Romiou Formation (Lapierre, 1975) or Dhiarrizos Group (Swarbrick & Robertson, 1980) and the Mamonia Formation (Lapierre, 1975) or Ayios Photios Group (Swarbrick & Robertson, 1980; Fig. 3). The Petra tou Romiou Formation is the lower tectonic unit and consists of volcanic rocks of mafic to felsic composition associated with Late Triassic pelagic and reefal sediments. The structurally overlying Mamonia Formation is predominantly formed of sedimentary rocks, which record the contemporaneous evolution of the basin from shallow to deep water environments (Lapierre & Rocci, 1970; Lapierre, 1975).

On the basis of petrological and major element chemistry, earlier workers (Lapierre, 1975; Lapierre & Rocci, 1976; Swarbrick & Robertson, 1980) have considered all the volcanic rocks of the Mamonia Complex as alkali basalts and their fractionated products. More recently, Malpas, Calon & Squires (1993) considered, on the basis of elemental chemistry, that more than 80 % of the Mamonia volcanic rocks are tholeiitic and exhibit N-MORB affinities. They concluded that most of the Late Triassic basalts represent preserved remnants of the Triassic oceanic crust, the main part of which was subducted beneath the Troodos microplate. According to Malpas, Calon & Squires (1993), the tholeiitic basalts of the Petra tou Romiou Formation are predominantly weakly pillowed lavas with interpillow voids and fractures filled with calcilutite, manganiferous cherts and often covered by radiolarian cherts, shale and minor calcilutite. The aphyric and highly porphyritic alkali basalts are associated with the same range of sedimentary rocks. The aphyric pillow basalts have abundant calcite- or zeolite-filled vesicles

https://doi.org/10.1017/S0016756806002937 Published online by Cambridge University Press

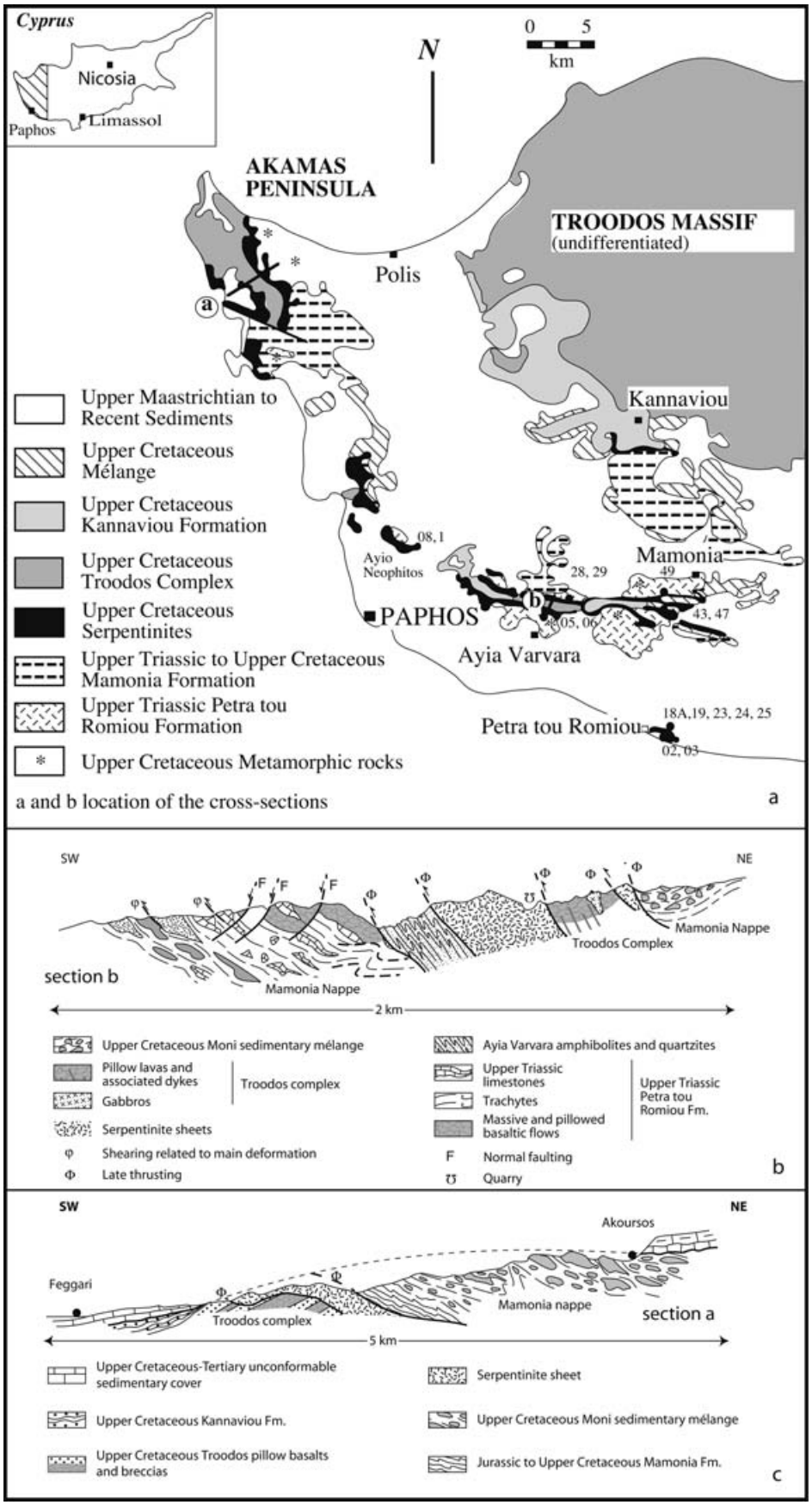

Figure 2. (a) Simplified geological map of Cyprus showing the location of the erosional windows of the Mamonia complex (based on the geological maps of Lapierre, 1975; Malpas, Xenophontos & Williams, 1992; Malpas, Calon & Squires, 1993). (b, c) Structural cross-sections along section lines in the Akamas peninsula (b) and Ayia Varvara (c) windows based on the geological maps of Lapierre (1975) and our own observations (this paper). The locations of the sections are shown in (a).

https://doi.org/10.1017/S0016756806002937 Published online by Cambridge University Press

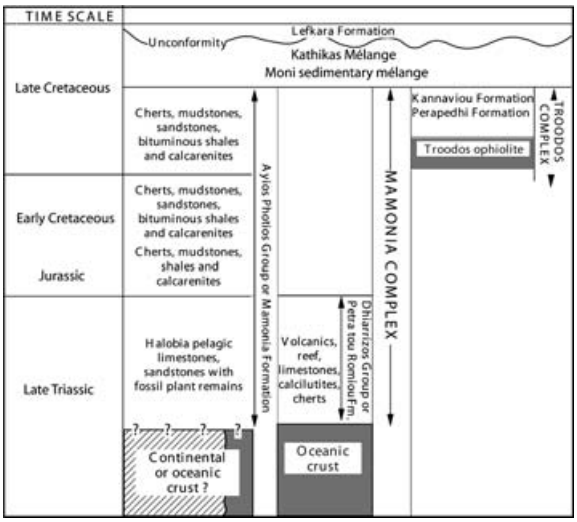

Figure 3. Simplified stratigraphic terminology of the Mesozoic rocks from Cyprus (after Lapierre, 1975; Swarbrick & Robertson, 1980; Malpas, Calon & Squires, 1993).

and rest upon the tholeiitic basalts. Clinopyroxene-phyric ankaramites, trachytes and phonolites are poorly exposed and represent less than 5 % of the Mamonia Complex volcanics.

The Mamonia Formation, the base of which is unknown, consists of sandstones with fossil plant remains, Halobia pelagic limestones stratigraphically overlain by a thick pile of radiolarian cherts, black spongolites interbedded with red and/or green clays, mudstones, siltstones and micritic limestones. Locally, bituminous shales (near Ayios Photios village) or green dark sandstones (Akamas peninsula) are interbedded within the radiolarian cherts. The age of the Mamonia Formation ranges from Late Triassic to Late Cretaceous (Bragin, Bragina & Krylov, 2000). Locally, alkali dolerite dykes and sills intrude the lowermost sandstones.

The Mamonia Complex is stratigraphically overlain successively by an olistostrome unit composed of metre- to kilometre-size blocks of the underlying rocks (Mamonia volcanics and sediments, Ayia Varvara metamorphic rocks, silicified serpentinites: Malpas, Xenophontos & Williams, 1992) set into a grey to pink argillaceous matrix (Moni Mélange and/or Kathikas Mélange: Swarbrick & Naylor, 1980) and by the gently deformed Late Cretaceous to Early Tertiary Lefkara Formation (Fig. 3).

The tectonic emplacement of the Mamonia Complex onto the Troodos Complex occurred after the deposition of the Late Cretaceous Kannaviou Formation and before that of the Late Cretaceous–Early Tertiary Lefkara Formation, that is, during Maastrichtian time (Lapierre, 1975; Robertson & Woodcock, 1982; Swarbrick, 1993). The nature of the collision of these two complexes remains a matter of debate. For Murton (1990) and Malpas, Calon & Squires (1993), the emplacement of the Mamonia nappes onto the Troodos Complex is due to a frontal collision between Troodos and a continental microplate located south of Cyprus. According to Malpas, Calon & Squires (1993), the continental margin rocks of the Mamonia Complex were delaminated from their basement upon arrival at a N-dipping subduction zone and emplaced onto the fore-arc region of the Troodos microplate. For Clube & Robertson (1986), McLeod (1990), Swarbrick (1993) and McLeod & Murton (1995), the emplacement of the Mamonia Complex and Troodos tectonic imbrication took place along transcurrent faults which affected the Troodos southwestern margin, the Limassol Forest and Akamas Peninsula, or along a fossil oceanic transform fault (E–W Arakapas–Athrakos Fault). More recently, Bailey, Holdsworth & Swarbrick (2000) have distinguished in the Mamonia Complex Suture three main tectonic events of Late Cretaceous age: (1) a high temperature (600 °C) transform-related, dextral strike-slip and localized metamorphism (Ayia Varvara Formation, 90–83 Ma), (2) retrograde hydration during dextral transtension associated with a rotation of the Cyprus microplate and the shallow level emplacement of serpentinites (83–73 Ma), and finally, (3) a regional contractional reactivation at low temperature which ended by the latest Maastrichtian (65 Ma). This deformation history is consistent with a model postulating that a Troodos microplate impinged on the Mamonia Complex during westerly- to southwesterly-directed plate motion, contractionally reactivating the weak suture zone.

3. Analytical procedures

Mineral analyses were carried out on the Cameca SX100 electron microprobe fitted with five wavelength spectrometers at the 'Service commun microsonde', University of Montpellier II. The standard working conditions were 20 kv and 10 nA, with a beam size of 1 μm and integrated counting times of 20–30 s. The accuracy of major element determinations is better than $\pm$ 1 % of the total value.

Major elements and compatible trace element analyses by ICP-Optical Emission Spectroscopy were done at the 'Centre de Recherche Pétrographiques et Géochimiques' (CRPG) in Nancy, on whole rocks powdered in an agate mill. Other trace elements, including the REE, were analysed by ICP-MS at the University Joseph Fourier in Grenoble, after acid dissolution of 100 mg sample, using the procedures of Barrat, Keller & Amossé (1996). Limits of detection are: REE and Y = 0.003 ppm, U, Pb and Th = 0.005 ppm, Hf and Nb = 0.01 ppm, Ta = 0.03 ppm, and Zr = 0.04 ppm. The standards used for the analyses were JB2, Bhvo-2, Bir-1 and UBn1. Analytical errors are 1–3 % for major elements and less than 3 % for trace elements.

Sr and Nd isotopic ratios were measured at the Laboratoire de Géochimie isotopique de l'Université Paul Sabatier de Toulouse on a Finnigan MAT261 multicollector mass spectrometer using the analytical

https://doi.org/10.1017/S0016756806002937 Published online by Cambridge University Press

procedures described by Lapierre *et al.* (1997). Results on La Jolla Nd standard yielded $^{143}Nd/^{144}Nd = 0.511850 \pm 0.000017$ (2σ external reproducibility, n = 12). Results on NBS 987 Sr standard yielded an average of $^{87}Sr/^{86}Sr = 0.710250 \pm 0.000030$ (2σ external reproducibility, n = 11). $^{87}Sr/^{86}Sr$ and $^{143}Nd/^{144}Nd$ were normalized for mass fractionation relative to $^{86}Sr/^{88}Sr = 0.1194$ and $^{146}Nd/^{144}Nd = 0.7219$, respectively. εNd_i calculated with actual $(^{143}Nd/^{144}Nd)_{CHUR} = 0.512638$ and $(^{147}Sm/^{144}Nd)_{CHUR} = 0.1967$. εSr_i calculated with actual $(^{87}Sr/^{86}Sr)_{CHUR} = 0.70450$ and $(^{87}Rb/^{86}Sr)_{CHUR} = 0.084$ (McCulloch & Wasserburg, 1978).

For lead separation, powdered samples were weighed to obtain approximately 200 ng of lead. With a view to remove possible effects of submarine alteration, samples were intensively leached with a HF + 6N HCl mixture for 30 minutes at 65 °C before acid dissolution and lead chemical separation. Such leaching experiments have been previously efficiently used to remove secondary alteration effects (e.g. Abouchami, Galer & Hofmann, 2000). Lead isotopes were analysed on a VG Plasma 54 multi-collector inductively coupled plasma-mass spectrometer (MC-ICP-MS) at the 'Ecole Normale Supérieure de Lyon'. Lead isotope compositions were measured using the Tl normalization method described by White, Albarède & Telouk (2000). For Pb isotope analysis, samples were bracketed between NIST 981 standards and calculated with respect to the value reported for this standard by Todt *et al.* (1996). This technique yields internal precision of ~ 50 ppm (2σ) and an external reproducibility of ~ 150 ppm (2σ for $^{206}Pb/^{204}Pb$ ratios, n = 20).

All the isotopic data have been corrected for *in situ* decay using an age of 210 Ma (Late Triassic) on the basis of the Norian–Carnian fauna found in the pelagic limestones.

4. Petrographic and chemical data

4.a. Sample selection and alteration

Fifteen samples were selected for petrological and geochemical investigations, based on petrographic type, the overall freshness of the volcanic rocks, and the type of sediments they are associated with. The location of analysed samples is shown in Figure 2a.

Whole rock major, trace element, and Nd, Sr and Pb isotopic chemistry of the Mamonia volcanic rocks are given in Tables 1 and 2. The high levels of loss of ignition (LOI) values are due to the abundance of calcite- or zeolite-filled vesicles. Because of the low-grade metamorphism which affects the Mamonia Complex volcanic rocks, Large Ion Lithophile Elements (LILE) known to be sensitive to alteration and metamorphism are not considered to be representative of the primary composition of these rocks. To test the behaviour of some incompatible trace elements during metamorphism, we have plotted La, Pb and Rb against Th considered as immobile during post-magmatic processes (Fig. 4). The majority of the Mamonia volcanics (with the exception of trachytes) exhibit a linear trend in the La and Pb v. Th plots (Fig. 4a, b), suggesting that these elements have not been extensively affected during the low-grade metamorphism experienced by the Mamonia rocks. In particular, in the Pb v. Th diagram (Fig. 4b) the samples define a line with a correlation factor of 0.76, which increases to 0.96 when removing the trachytes from the calculation. This feature suggests that Pb remains almost immobile in all the samples studied except in the trachytes. In contrast, the scattering of Mamonia samples observed in the Rb v. Th diagram is related to Rb mobility during low-grade metamorphism (Fig. 4c).

Because this low-grade metamorphism modified the bulk major element chemistry, the various types among the Mamonia volcanic rocks have been discriminated using Ti and immobile trace elements Zr, Nb and Y (Fig. 5a). Cr spinel–olivine basalts plot at the boundary of fields 3 and 5. Intersertal plagioclase and clinopyroxene basalts cluster in the alkali basalt field, but the porphyritic volcanic rocks show an evolution towards more evolved facies (hawaiites and mugearites). One basaltic sample with intersertal texture (CY01-29) plots near the limit between alkali and sub-alkali basalts (Fig. 5a). Four groups have been therefore distinguished based on the texture, mineralogy and trace element chemistry:

Type 1 – depleted tholeiites represented by Cr-spinel (CY01-49) and olivine-bearing basalts (CY01-08, CY01-10);

Type 2 – oceanic island tholeiite represented by intersertal basalt CY01-29;

Type 3 – alkali basalts including two intersertal lavas (CY01-05, CY01-06) and the olivine-, plagioclase- and clinopyroxene-phyric basalts and hawaiites (CY01-02, CY01-19, CY01-25, CY01-28, CY01-43, CY01-47);

Type 4 – trachytes (CY01-03, CY01-18A, CY01-23, CY01-24).

4.b. Major and trace elements

4.b.1. Type 1 – depleted tholeiites

These pillowed basalts are associated with or stratigraphically overlain by red radiolarian cherts and pink pelagic limestones. They show quenched margins and variolitic textures. They consist of skeletal (< 1 mm) olivine phenocrysts pseudomorphed into celadonite, calcite or chalcedony, embedded in a fine-grained matrix, which contains plagioclase and clinopyroxene. Olivine often includes euhedral Ti-free brown spinels, with rather high Cr no. (Cr/Cr+Al) and Mg no. (Mg/Mg+Fe).

The Cr-spinel and olivine basalts have the highest Ni contents and the lowest abundances in Ti (Fig. 5b), incompatible elements (Zr, Hf, Nb, Ta, Th, Y) and

https://doi.org/10.1017/S0016756806002937 Published online by Cambridge University Press

Table 1 Major and trace element composition (in wt %, and ppm, respectively) of the Mamonia volcanic rocks

Sample	CY01-08 (Type 1)	CY01-10 (Type 1)	CY01-49 (Type 1)	CY01-29 (Type 2)	CY01-02 (Type 3)	CY01-05 (Type 3)	CY01-06 (Type 3)	CY01-19 (Type 3)	CY01-25 (Type 3)	CY01-28 (Type 3)	CY01-43 (Type 3)	CY01-47 (Type 3)	CY01-03 (Type 4)	CY01-18 (Type 4)	CY01-23 (Type 4)	CY01-24 (Type 4)
SiO_2	47.55	45.47	51.30	49.06	44.92	47.73	49.12	51.10	47.66	48.83	48.79	51.40	60.70	66.50	67.17	68.98
TiO_2	1.16	1.51	0.74	1.87	3.66	1.75	1.69	1.71	3.05	3.06	2.32	2.39	0.52	0.49	0.21	0.35
Al_2O_3	15.90	16.10	14.54	13.87	15.23	16.13	16.96	18.39	13.36	18.05	14.92	18.52	16.14	10.61	12.92	9.49
Fe_2O_3*	9.89	12.50	9.02	13.65	13.29	10.34	10.00	8.83	8.71	8.88	8.90	11.62	5.85	7.20	4.51	11.14
MnO	0.17	0.27	0.14	0.21	0.36	0.17	0.16	0.15	0.30	0.23	0.29	0.32	0.18	0.41	0.16	0.44
MgO	7.38	4.50	4.15	6.42	6.13	5.20	7.10	5.93	2.06	5.53	1.83	1.91	2.96	0.31	1.34	0.46
CaO	13.38	14.38	16.51	1.11	10.22	13.08	9.96	6.72	8.60	9.01	13.26	5.57	4.94	4.14	4.69	1.43
Na_2O	3.92	4.52	3.49	3.45	3.23	3.00	4.70	5.71	3.41	5.80	4.85	4.74	4.76	4.69	4.65	3.39
K_2O	0.49	0.56	nd	0.19	1.96	2.37	0.12	1.14	2.13	1.18	4.01	2.70	3.80	5.58	4.32	4.25
P_2O_5	0.13	0.17	0.06	0.18	0.41	0.21	0.20	0.31	0.67	0.41	0.92	0.81	0.09	0.06	0.00	0.05
LOI	8.11	10.19	5.88	5.09	5.50	9.46	5.81	5.07	11.26	8.76	9.96	5.13	11.43	4.08	6.58	3.77
Total	99.79	99.83	99.84	99.85	99.87	99.82	100.02	99.9	99.88	99.89	99.9	99.95	99.86	99.95	99.86	99.91
V	277.0	342.0	207.0	375.0	398.0	267.0	316.0	191.0	189.0	522.0	97.0	70.0	1.0	2.0	2.0	
Cr	610.0	458.0	467.0	95.0	32.0	44.0	62.0	165.0	6.0	67.0	5.0	1.0	2.0	7.0	8.0	5.0
Ni	240.0	228.0	168.0	55.0	27.0	67.0	60.0	66.0	1.0	46.0	2.0	0.0	2.0	0.0	3.0	6.0
Co	45.59	51.26	47.31	46.58	41.04	46.09	41.18	24.30	14.92	44.63	14.41	7.12	6.40	1.28	2.68	6.29
Cs	0.09	0.33	0.03	0.15	0.03	0.96	0.10	0.20	0.69	0.69	0.15	0.31	0.07	0.08	0.19	0.07
Rb	4.17	10.80	0.53	2.13	16.37	25.98	1.59	16.88	29.52	19.58	33.79	44.22	37.61	89.30	97.70	99.47
Sr	145.43	254.56	97.17	238.33	441.14	215.00	716.27	375.04	522.93	317.27	314.80	642.77	58.29	66.68	73.48	80.87
Ba	26.69	58.35	16.46	179.57	475.71	63.53	62.76	385.46	304.43	362.33	670.05	799.27	662.98	475.68	248.08	98.32
U	0.07	0.17	0.06	0.27	1.03	0.42	0.37	1.07	1.42	1.16	3.40	2.34	2.88	5.18	2.83	2.91
Th	0.18	0.12	0.12	0.68	3.90	1.57	1.47	4.55	4.37	3.86	6.27	8.43	13.13	15.89	19.89	29.22
Pb	0.40	0.37	0.16	0.44	1.96	0.99	1.28	1.82	1.77	1.74	2.80	4.28	2.07	12.61	7.91	10.30
Hf	1.85	2.38	1.22	3.02	4.84	2.70	2.65	5.54	6.05	4.59	6.81	7.33	20.02	18.96	21.89	22.97
Zr	71.51	96.11	45.74	117.82	223.03	110.93	112.52	264.84	281.69	209.51	345.07	412.04	907.94	891.65	984.51	1060.82
Ta	0.16	0.11	0.08	0.57	3.55	1.29	1.20	3.13	4.08	3.14	5.445	4.28	10.09	11.96	12.68	20.13
Nb	2.51	1.74	1.30	9.47	61.28	20.82	21.00	53.05	67.33	53.75	99.26	125.25	193.91	199.08	207.99	275.41
Y	27.09	34.97	19.47	37.45	32.43	25.32	24.45	29.59	33.70	24.72	39.59	40.40	78.65	86.66	101.57	110.05
La	2.56	2.78	1.76	7.74	36.02	13.56	12.58	32.85	43.67	30.34	64.28	72.53	99.21	82.87	130.35	198.24
Ce	7.30	8.78	4.52	18.41	74.40	29.86	27.23	66.29	92.06	64.28	125.06	144.67	197.52	161.46	255.77	390.11
Pr	1.31	1.62	0.84	2.75	9.21	3.77	3.67	7.99	11.45	7.98	14.87	17.17	23.59	18.02	28.81	45.70
Nd	7.06	9.35	4.76	13.77	37.49	15.86	15.86	31.76	46.32	31.23	57.78	64.78	84.16	66.47	100.58	171.07
Sm	2.50	3.22	1.67	4.11	7.59	3.81	3.66	6.47	9.31	6.47	10.93	11.97	15.71	13.22	19.70	30.37
Eu	0.95	1.24	0.66	1.44	2.39	1.34	1.33	2.07	2.83	1.92	3.45	4.37	3.10	2.89	1.95	5.85
Gd	3.49	4.57	2.40	5.22	7.23	4.30	4.07	6.34	8.21	5.89	10.12	10.34	13.81	12.92	17.44	26.29
Tb	0.65	0.83	0.45	0.96	1.03	0.72	0.69	0.91	1.18	0.86	1.31	1.47	2.17	2.26	3.00	3.78
Dy	4.16	5.38	2.96	5.95	5.73	4.37	4.16	5.24	6.24	4.69	7.32	7.71	12.96	13.87	17.26	20.74
Ho	0.92	1.14	0.66	1.31	1.09	0.88	0.83	1.03	1.19	0.89	1.41	1.49	2.72	2.99	3.55	4.00
Er	2.71	3.38	1.99	3.72	2.92	2.54	2.37	2.74	3.20	2.40	3.66	3.97	8.19	8.36	10.15	10.61
Yb	2.47	3.18	1.87	3.44	2.38	2.30	2.17	2.34	2.68	2.06	3.04	3.44	7.96	7.76	9.32	10.12
Lu	0.37	0.47	0.28	0.53	0.34	0.32	0.31	0.37	0.37	0.29	0.44	0.49	1.21	1.22	1.31	1.47

(Fe_2O_3* is total iron presented as Fe_2O_3).

Table 2 Sr, Nd and Pb isotopic composition of the Mamonia volcanic rocks

Sample	CY01-08 (Type 1)	CY01-10 (Type 1)	CY01-49 (Type 1)	CY01-29 (Type 2)	CY01-02 (Type 3)	CY01-05 (Type 3)	CY01-06 (Type 3)	CY01-19 (Type 3)
$^{87}Sr/^{86}Sr$	0.705892 ± 14	0.705978 ± 9	0.705429 ± 08	0.704224 ± 08	0.703453 ± 10	0.705245 ± 9	0.704389 ± 10	0.703867 ± 17
$^{87}Rb/^{86}Sr$	0.0833005	0.12276	0.015777	0.0258122	0.107313	0.1452693	0.006461	0.1301933
$(^{87}Sr/^{86}Sr)_i$	0.705644	0.705611	0.7053815	0.704146	0.703133	0.704201	0.70437	0.703477
$^{143}Nd/^{144}Nd$	0.513046 ± 14	0.513013 ± 11	0.512937 ± 12	0.513012 ± 11	0.512739 ± 8	0.512847 ± 9	0.512798 ± 10	0.512758 ± 9
$^{147}Sm/^{144}Nd$	0.214619	0.208133	0.212126	0.180638	0.1225208	0.1452693	0.1394371	0.123245
$(^{143}Nd/^{144}Nd)_i$	0.512751	0.512727	0.512645	0.512764	0.5125706	0.5126474	0.5126064	0.512589
εNd	7.48	7.01	5.42	7.73	3.96	5.46	4.66	4.31
$^{206}Pb/^{204}Pb$	18.98	19.27	19.44	20.91	21.59	20.49	19.98	21.42
$^{238}U/^{204}Pb$	10.48	28.40	22.18	40.94	35.43	28.12	18.99	39.95
$(^{206}Pb/^{204}Pb)i$	18.64	18.33	18.71	19.55	20.42	19.56	19.35	20.10
$^{207}Pb/^{204}Pb$	15.55	15.55	15.59	15.69	15.76	15.67	15.62	15.75
$^{235}U/^{204}Pb$	0.08	0.21	0.16	0.30	0.26	0.21	0.14	0.29
$(^{207}Pb/^{204}Pb)i$	15.53	15.50	15.56	15.62	15.70	15.62	15.58	15.69
$^{208}Pb/^{204}Pb$	38.59	38.46	38.82	40.01	41.19	40.31	39.83	41.26
$^{232}Th/^{204}Pb$	30.16	21.82	47.78	105.73	138.98	108.03	77.04	175.02
$(^{208}Pb/^{204}Pb)i$	38.27	38.23	38.32	38.90	39.72	39.17	39.02	39.41

Table 2 *Continud.*

Sample	CY01-25 (Type 3)	CY01-28 (Type 3)	CY01-43 (Type 3)	CY01-47 (Type 3)	CY01-03 (Type 4)	CY01-18A (Type 4)	CY01-23 (Type 4)	CY01-24 (Type 4)
$^{87}Sr/^{86}Sr$	0.703409 ± 2	0.705021 ± 19	0.705698 ± 8	0.703586 ± 10	0.706854 ± 10			0.824443 ± 16
$^{87}Rb/^{86}Sr$	0.1632695	0.17846	0.3104769	0.198957	1.866602			3.59938
$(^{87}Sr/^{86}Sr)_i$	0.702922	0.704488	0.7047703	0.702991	0.701275			0.813684
$^{143}Nd/^{144}Nd$	0.512864 ± 15	0.512739 ± 10	0.512697 ± 6	0.512705 ± 21	0.512683	0.512675 ± 10	0.512715 ± 6	0.512726 ± 6
$^{147}Sm/^{144}Nd$	0.121508	0.125158	0.114395	0.111755	0.112878	0.120226	0.11475	0.107345
$(^{143}Nd/^{144}Nd)_i$	0.512697	0.512567	0.51254	0.512551	0.512527	0.51251	0.512557	0.512578
εNd	6.43	3.89	3.36	3.59	3.13	2.77	3.7	4.11
$^{206}Pb/^{204}Pb$	21.77		22.77	20.75	22.27	20.88	20.78	20.72
$^{238}U/^{204}Pb$	54.42		83.42	36.33	97.86	27.39	24.96	18.95
$(^{206}Pb/^{204}Pb)i$	19.96		20.00	19.55	19.02	19.97	19.95	20.09
$^{207}Pb/^{204}Pb$	15.78		15.82	15.70	15.82	15.74	15.72	15.72
$^{235}U/^{204}Pb$	0.40		0.61	0.27	0.71	0.20	0.18	0.14
$(^{207}Pb/^{204}Pb)i$	15.69		15.68	15.64	15.66	15.70	15.68	15.68
$^{208}Pb/^{204}Pb$	41.12		41.06	40.57	43.57	40.69	41.25	41.55
$^{232}Th/^{204}Pb$	172.76		158.85	135.2	461.38	86.74	196.56	196.97
$(^{208}Pb/^{204}Pb)i$	39.30		39.39	39.15	38.70	39.78	39.18	39.47

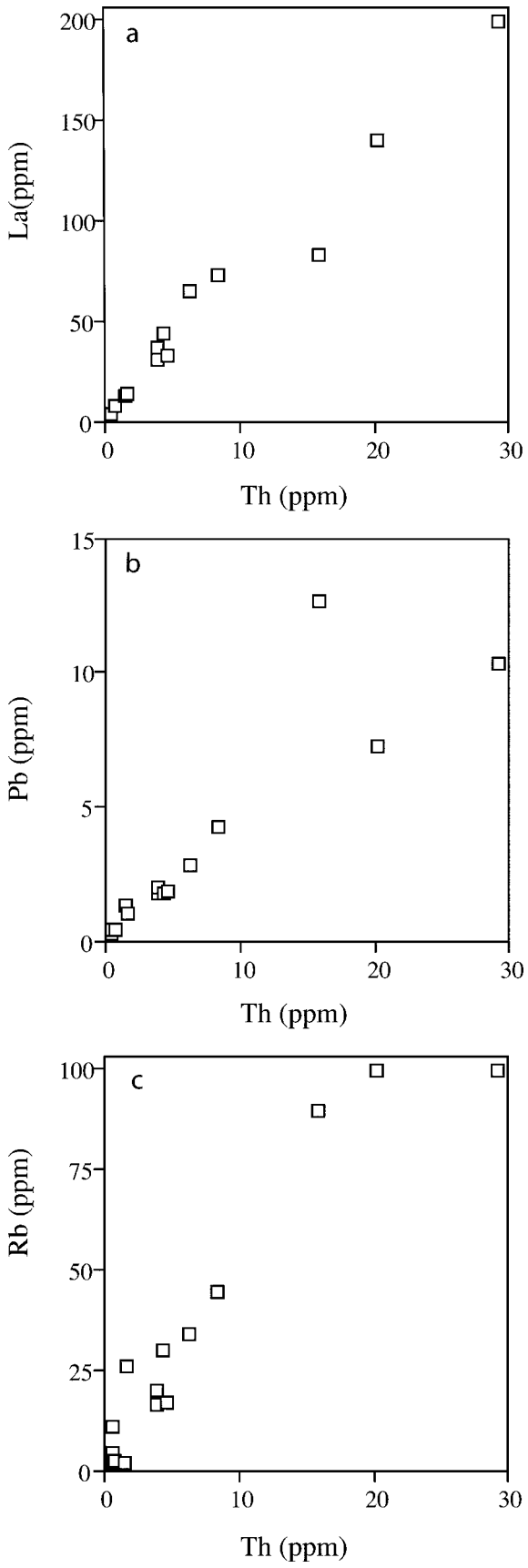

Figure 4. (a) La (ppm) v. Th (ppm), (b) Pb (ppm) v. Th (ppm), (c) Rb (ppm) v. Th (ppm) plots for the Mamonia volcanic rocks. The correlation factor calculated for the Pb v. Th regression line (b) does not integrate the trachytic samples.

Rare Earth Elements (REE) (Fig. 6a, b). Olivine basalts are characterized by depleted Light REE (LREE) patterns ($0.63 < (La/Yb)_N < 0.74$). The primitive mantle-normalized (Sun & McDonough, 1989) multi-element plots of these olivine basalts show Th and Pb negative anomalies and no enrichment or depletion in Nb and Ta relative to LREE (Fig. 6b). Such features are characteristic of N-MORB. These basalts have then been classified as depleted tholeiites or Type 1 tholeiites.

4.b.2. Type 2 – oceanic island tholeiite (OIT)

Sample CY01-29 was collected in a pillowed flow associated with pink calcilutite. It consists of andesine ($An_{32–49}$) laths embedded by augite ($Wo_{35–44}En_{36–46}Fs_{13–23}$) and late crystallized titanomagnetite. This basalt shows a flat to slightly enriched REE pattern ($(La/Yb)_N = 1.6$) (Fig. 6a). Its primitive mantle-normalized multi-element plot (Fig. 6b) displays features of transitional (T)-MORB or oceanic island tholeiite (OIT).

4.b.3. Type 3 – alkali basalts

Alkali intersertal basalts are mostly found as pillows and hyaloclastites capped by pink calcilutite (CY01-05), which also fill interpillow voids and fractures. Less often, they occur as massive flows associated with white reefal limestones (CY01-06). They consist of plagioclase laths embedded by clinopyroxene and late crystallized titanomagnetite. Plagioclase is often replaced by albite or zeolites. When preserved, it shows a labradorite ($An_{50–55}$) composition. The clinopyroxene is a Mg-rich augite ($Wo_{35–44}En_{37–46}Fs_{13–24}$) which exhibits Fe-enrichment both from core to rim within a single crystal and from phenocrysts to microcrysts. The sequence of crystallization of these two basalts (olivine–plagioclase–clinopyroxene–magnetite) is that of a tholeiite, but their trace element chemistry is close to that of mildly alkaline rocks.

The other alkali basalts are porphyritic, with abundant centimetre-sized plagioclase phenocrysts, with the exception of samples CY01-47 and CY01-43 which are aphyric. CY01-43 was sampled in a dyke intruding the pillowed flows. The porphyritic volcanic rocks commonly contain calcite-, celadonite-, prehnite- and/or zeolite-filled vesicles. Their groundmass is composed of abundant plagioclase microlites, clinopyroxene microphenocrysts, acicular ilmenite and titanomagnetite. Frequently, TiO_2-rich oxides are rimmed by late-magmatic biotite. Preserved (anorthoclase: $Ab_{76}Or_{23}$) or altered (adularia: $Ab_{1–2}Or_{98–99}$) alkali feldspar microlites may occur in the groundmass. When present, olivine is systematically replaced by serpentine, smectite or less frequently by anthophyllite or calcite. Plagioclase phenocrysts are zoned with bytownite ($An_{82–85}$) or labradorite ($An_{54–64}$) cores and labradorite ($An_{52–62}$) or andesine ($An_{30–49}$) rims. Clinopyroxene phenocrysts are diopside ($Wo_{45–47}En_{36–41}Fs_{9–18}$)

https://doi.org/10.1017/S0016756806002937 Published online by Cambridge University Press

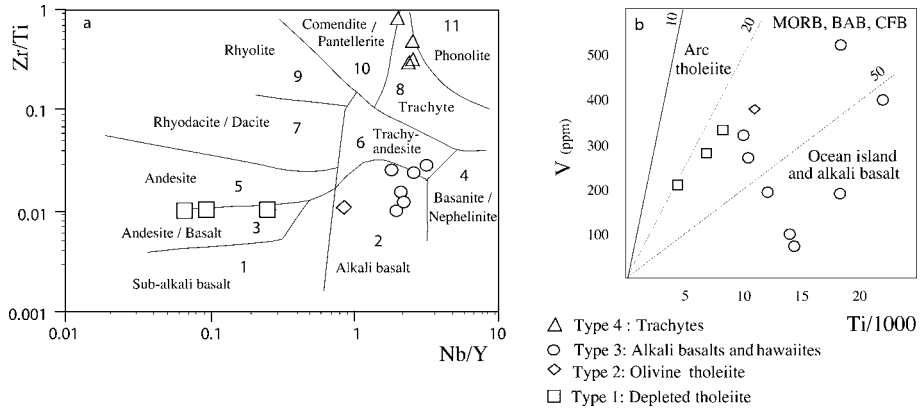

Figure 5. (a) Zr/Ti v. Nb/Y and (b) V (ppm) v. Ti/1000 plots of the Mamonia volcanic rocks. Fields are after Winchester & Floyd (1977) and Shervais (1982).

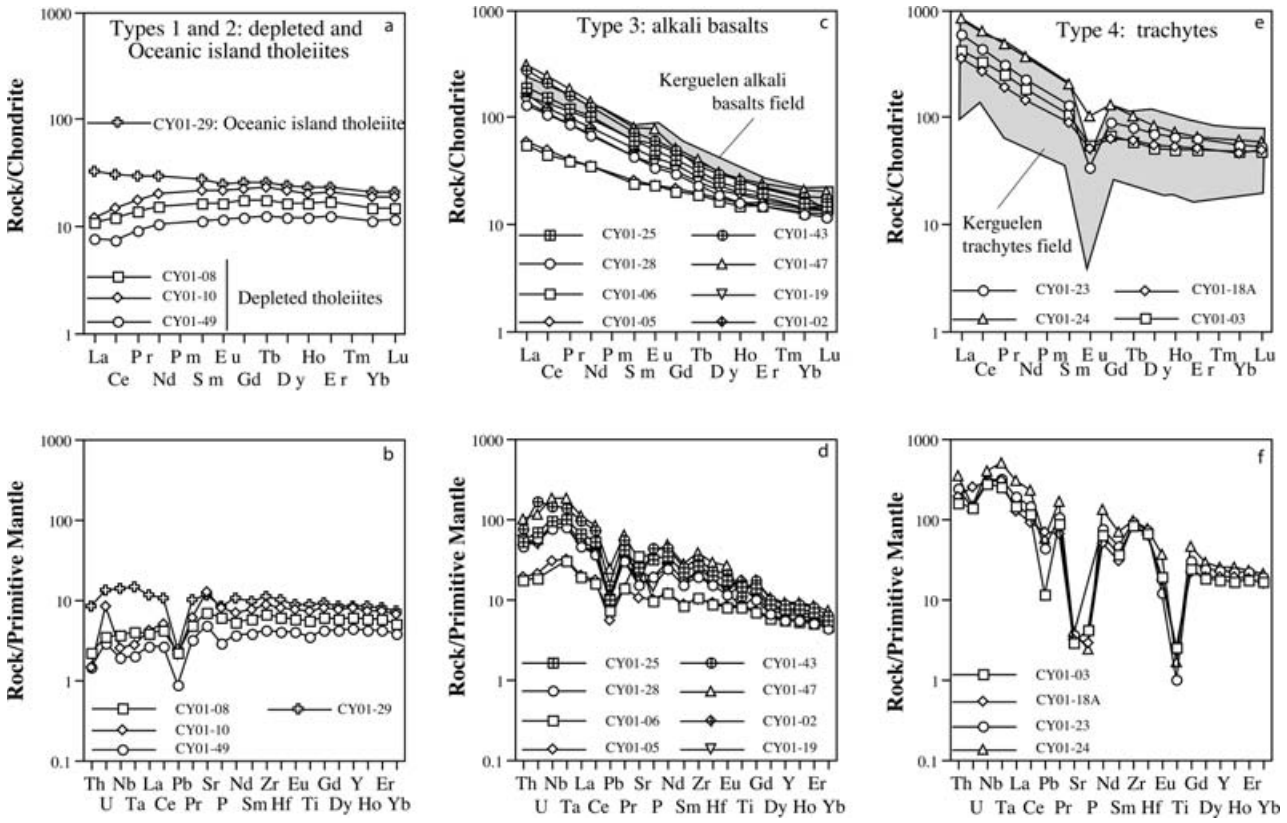

Figure 6. Chondrite-normalized Rare Earth Element patterns and primitive mantle-normalized multi-element plots of: (a, b) the Mamonia tholeiites; (c, d) the Mamonia alkali basalts; (e, f) the Mamonia trachytes. The grey fields indicated in (c) and (e) correspond to the Kerguelen alkali basalts and trachytes domain and are shown for comparison (data are from Kieffer, Arndt & Weiss, 2002). Normalization values from Sun & McDonough (1989).

evolving towards pink TiO_2-rich (1.6 to 3.7 %) augite ($Wo_{42–45}En_{37–34}Fs_{14–19}$). CY01-47 and CY01-4 are characterized by a seriate texture marked by fluidal plagioclase laths and/or microlites. The occurrence of late magmatic biotite suggests the presence of water in this magma.

Type 3 basalts show high TiO_2 contents (Fig. 5b, Table 1). The Cr contents of the porphyritic basalts are significantly higher than those of the volcanic rocks with seriate and intersertal textures. Type 3 basalts have enriched LREE patterns ($4.2 < (La/Yb)_N < 15.16$; Fig. 6c) and are enriched in incompatible elements. Their primitive-mantle normalized multi-element plots are typical of alkalic mafic lavas with positive Th, Nb, Ta and Ti anomalies (Fig. 6d). Samples CY01-47 and CY01-43 differ from the other rocks by their negative Ti anomaly, which may be attributed to separation of Ti-rich magnetite; this suggests they represent the most fractionated rocks. Samples CY01-05 and CY01-06 differ by their lower $(La/Yb)_N$ ratios and abundances

https://doi.org/10.1017/S0016756806002937 Published online by Cambridge University Press

of most incompatible elements. They display mildly alkaline features and could therefore represent a transition between the ocean island tholeiite and the alkali basalts.

4.b.4. Type 4 – trachytes

The mode of occurrence of the trachytes (CY 01-03, 01-18A, 01-23, 01-24) is difficult to determine because most of our samples come from loose blocks of the Moni and/or Kathikas olistostromes, or from slivers caught within the thrust faults. However, when mapping the Paphos-Polis area in the early seventies, one of us (Lapierre, 1975) observed that the trachytes formed either small columnar-jointed flows resting on the pillows or dykes cutting the extrusive rocks. Light green or yellow in colour, the trachytes are alkali feldspar-phyric and seriate textured (CY01-23 and CY01-24) or aphyric and flow-banded with abundant flattened vesicles (CY01-03). When preserved, alkali feldspar has an anorthoclase ($Ab_{60–64}Or_{35–39}$) or sanidine composition. Na-rich clinopyroxene replaced by chlorite occurs in most rocks.

Trachytes are the most fractionated rocks of the Mamonia Complex as shown by their very low contents in compatible elements, Cr, Ni and V (Table 1). They are very LREE-enriched with $(La/Yb)_N$ ratio ranging between 9 and 14. Their REE patterns (about 1000 times the chondritic abundances; Fig. 6e) exhibit a marked negative Eu anomaly ($0.96 \geq Eu/Eu^* \geq 0.32$), indicative of significant plagioclase removal. Their primitive mantle-normalized (Sun & McDonough, 1989) spidergrams show Pb, Sr, P and Ti negative anomalies, which can be attributed to plagioclase, apatite and magnetite removal (Fig. 6f).

4.c. Isotopes

Reported in the εNd_i v. $^{206}Pb/^{204}Pb_i$ diagram (Fig. 7a), Type 1 tholeiites differ from N-MORB by lower εNd_i values ($+5.4 < \varepsilon Nd_i < +7.5$). They show the least Pb radiogenic isotopic composition and the higher $^{87}Sr/^{86}Sr_i$ ratios of the Mamonia volcanics (Table 2). In the $^{207}Pb/^{204}Pb_i$ v. $^{206}Pb/^{204}Pb_i$ diagram (Fig. 7b), they plot in the MORB-field and along the North Hemisphere Reference Line (NHRL: Zindler & Hart, 1986).

The εNd_i value of Type 2 tholeiite (+7.7) (Table 2; Fig. 7a) is the highest of the Mamonia volcanic suite and in the same range as those of the depleted tholeiites. In contrast to Type 1 tholeiites, the initial Pb isotopic ratios of sample CY01-29 are significantly higher and similar to those of some alkali basalts (Fig. 7a, b and next Section). The $^{87}Sr/^{86}Sr_i$ of this sample is slightly lower than those of the depleted tholeiites (Table 2).

The εNd_i of Type 3 span a large range of values (from +3.4 to +6.4) and fall in the field of OIB (Fig. 7a). The enriched character of the Type 3 mantle source is confirmed by the $^{206}Pb/^{204}Pb$ ratio, which is the highest of all the Mamonia volcanic rocks (Fig. 7b).

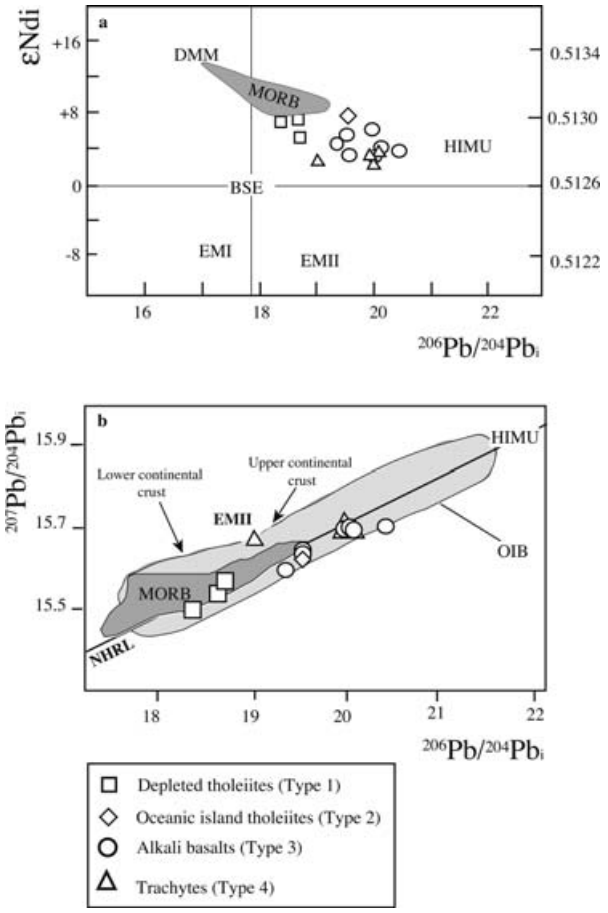

Figure 7. (a) εNd_i v. $(^{206}Pb/^{204}Pb)_i$ and (b) $(^{207}Pb/^{204}Pb)_i$ v. $(^{206}Pb/^{204}Pb)_i$ correlation diagrams showing that the Mamonia Upper Triassic volcanics were derived from the melting of enriched OIB type mantle sources. Mantle reservoirs are from Zindler & Hart (1986): Depleted MORB Mantle (DMM), Enriched Mantle 1 (EM1), Enriched Mantle 2 (EM2), High $\mu = ^{238}U/^{204}Pb$ (HIMU). The bulk silicate Earth value (BSE) is from Allègre, Lewin & Dupré (1988). NHRL = Northern Hemisphere Reference Line (Th/U = 4.0) has been defined by Zindler & Hart (1986).

The Type 4 rocks share with the alkali basalts similar εNd_i values and isotopic Pb ratios. One trachyte (sample CY01-03) differs from the others by its significantly lower $^{206}Pb/^{204}Pb_i$ (Table 2; Fig. 7a, b).

In summary, the Late Triassic Mamonia volcanism ranges from depleted olivine-tholeiites to trachytes through intersertal and plagioclase-clinopyroxene-phyric alkali basalts and oceanic island tholeiites. Depleted olivine basalts are associated with radiolarian cherts while most pelagic limestones and cherts are found interbedded with alkali basalts. Low-grade hydrothermal alteration, characterized by the presence of albite ± adularia ± celadonite ± prehnite ± smectites ± zeolites ± calcite ± chalcedony, variably affects all the rock types. The whole Mamonia suite displays geochemical features of within-plate magmatism.

https://doi.org/10.1017/S0016756806002937 Published online by Cambridge University Press

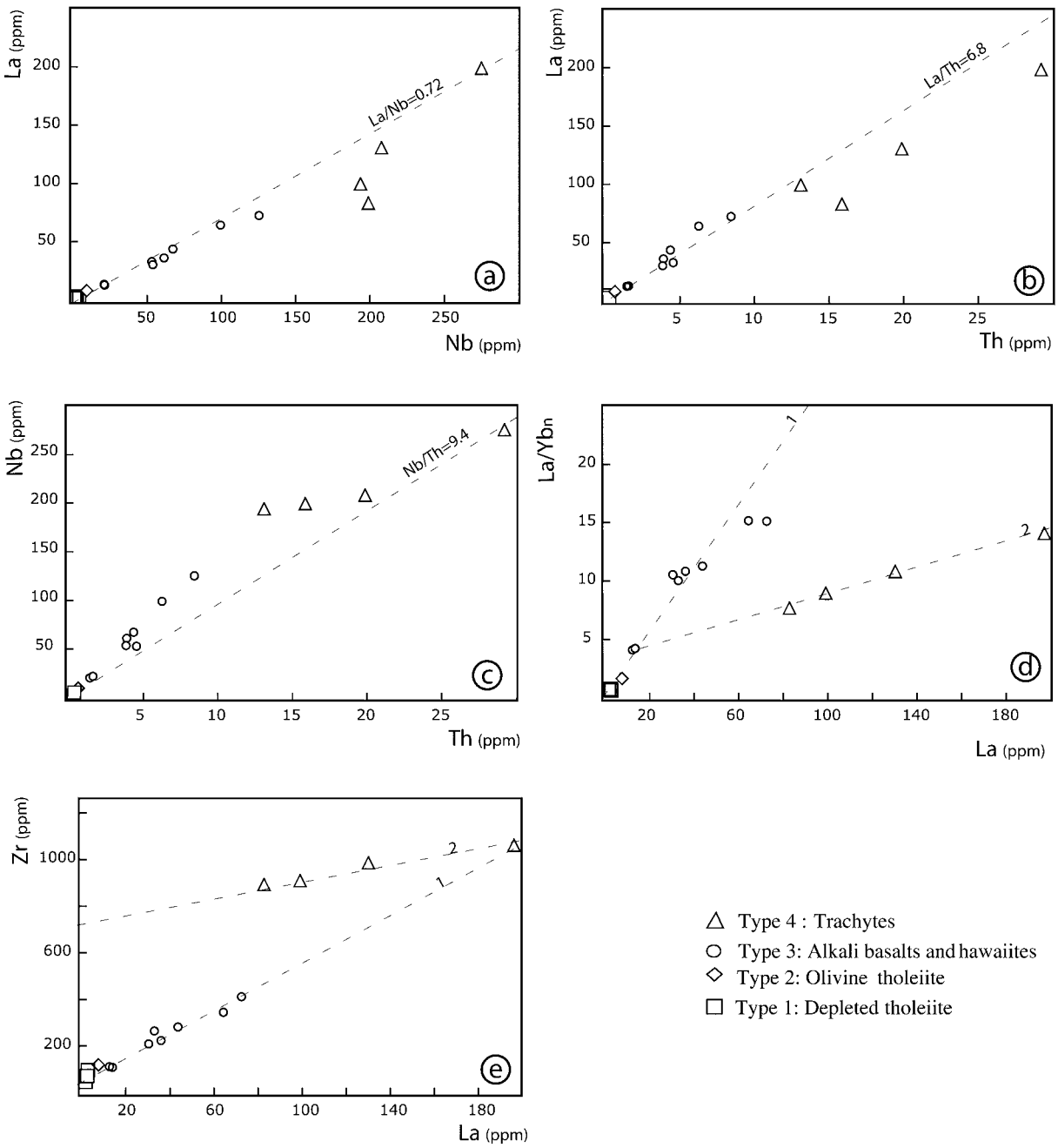

Figure 8. Incompatible trace element plots showing the geochemical relations between the four types of Mamonia volcanic rocks: (a) La (ppm) v. Nb (ppm), (b) La (ppm) v. Th (ppm), (c) Nb (ppm) v. Th (ppm), (d) La/Yb_N v. La (ppm), (e) Zr (ppm) v. La (ppm).

5. Discussion

5.a. Geochemical relationships between the four volcanic types

Mamonia mafic volcanic rocks exhibit positive correlation trends in the La–Nb, La–Th, Nb–Th and Zr–La diagrams (Fig. 8a–c, e). The trachytes do not fall within these trends, except sample CY01-24. This evolution from the depleted tholeiites towards the most enriched alkali basalts and one trachyte may be attributed to a temporal decrease in the degree of partial melting, assuming a homogeneous mantle source. However, in the Zr–La diagram only one trachyte plots on the tholeiite–basalt trend (line 1, slope Zr/La = 5.2). On the same diagram, the four trachytes alone define another trend (line 2, slope of 1.5). Similarly, in the La/Yb v. La diagram (Fig. 8d), the Mamonia volcanic rocks clearly exhibit two different trends: a steep positive line (Trend 1) defined by samples of Type 1, 2 and 3 (slope equal to 0.3); and a second trend (Trend 2 with a slope equal to 0.05) cross-cutting Trend 1 at the level of the less-enriched alkaline basalt (CY01-5). The presence of

https://doi.org/10.1017/S0016756806002937 Published online by Cambridge University Press

two distinctive trends suggests that the Mamonia mafic and felsic rocks are not linked together by crystal fractionation. This is a common feature observed in recent within-plate oceanic island volcanoes (Nuku Hiva island, Marquesas, French Polynesia: Legendre *et al.* 2005). The trachytes display patterns with highly fractionated MREE and Ti, Sr and Pb negative anomalies. These features are consistent with strong fractionation of amphibole, Fe–Ti oxides, apatite and plagioclase. Indeed, these minerals incorporate Ti (amphibole and/or Fe–Ti oxides) and LREE, Sr and Pb (apatite and plagioclase). The trachytes could derive from the partial melting at depth of mafic material which shares with the most differentiated alkali basalts similar Nd and Pb isotopic compositions (Fig. 7a, b). In contrast, the tholeiites and less-evolved alkali volcanic rocks display more varied geochemical features and were probably derived from heterogeneous enriched mantle sources.

5.b. Nature of the mantle sources

Sr initial isotopic ratios may not be used to characterize the magmatic signature of the studied volcanic rocks, considering the mobility of Rb during the submarine alteration processes (Fig. 4c). The Pb initial isotopic ratios have been tentatively used to characterize the composition of the mantle sources, considering that (1) Pb and Th (and to a lesser extent, U) contents have not been significantly modified by the submarine alteration (see the correlation between Pb and Th in Fig. 4b) and (2) the whole-rock powders have been thoroughly leached before Pb separation to remove any trace of superficial alteration (refer to Section 3).

In the εNd_i and $(^{207}Pb/^{204}Pb)_i$ v. $(^{206}Pb/^{204}Pb)_i$ diagrams (Fig. 7a, b), the Mamonia volcanic rocks exhibit a trend extending from the depleted MORB to the HIMU field, except trachyte (CY01-18), which plots in the $(^{207}Pb/^{204}Pb)_i$ v. $(^{206}Pb/^{204}Pb)_i$ diagram at the boundary between the EMII and OIB fields. This observation suggests that the Mamonia volcanic suite derived from the mixing between a depleted MORB source and a HIMU enriched source. None of the εNd_i values of the Mamonia volcanic rocks falls within the MORB field, not even the two tholeiitic basalts (CY01-29 and CY01-08) which display the highest εNd_i values (+7.7 and +7.4, respectively; Table 2). Similarly, the curvilinear trend displayed by the Mamonia volcanic suite in the εNd_i v. Nb and $(La/Yb)_N$ plots (Fig. 9a, c) suggests that this suite was derived from the mixing of a depleted source and a Nb- and Th-enriched component. This enriched component could be a HIMU mantle type.

Figure 10a and b illustrate a model that likely explains the variations of the Mamonia Nd and Pb initial isotopic ratios. In the $^{207}Pb/^{204}Pb$ v. $^{206}Pb/^{204}Pb$ diagram (Fig. 10b), the studied volcanic rocks (with the exception of the trachytic sample CY 01-24) plot along the mixing line (A) between the DMM and HIMU fields. The depleted tholeiites (Type 1) are less contaminated by the HIMU component while most of the alkali basalts and hawaiites and three out of four trachytes contain a higher imprint of a HIMU component. The

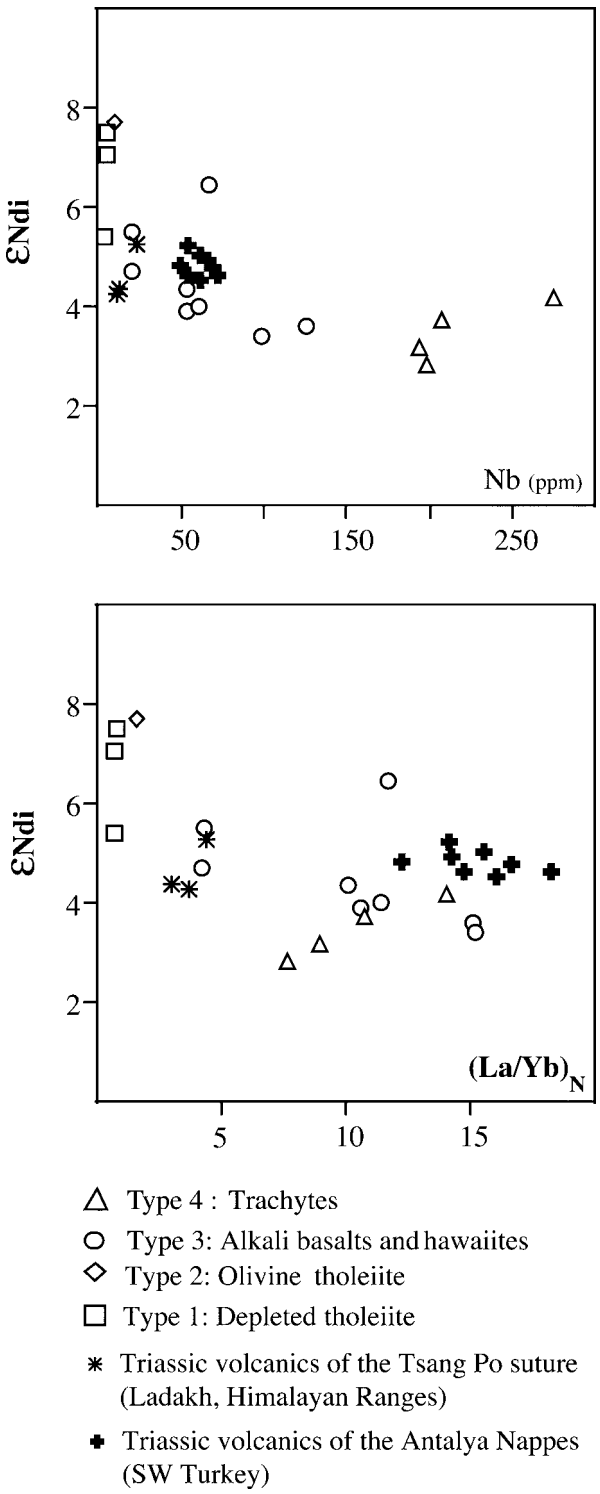

Figure 9. (a) εNd_i v. Nb (ppm), (b) εNd_i v. Th (ppm), (c) εNd_i v. $(La/Yb)_N$ correlation diagrams showing that the Upper Triassic Mamonia volcanic rocks derived from the melting of enriched OIB type mantle sources.

https://doi.org/10.1017/S0016756806002937 Published online by Cambridge University Press

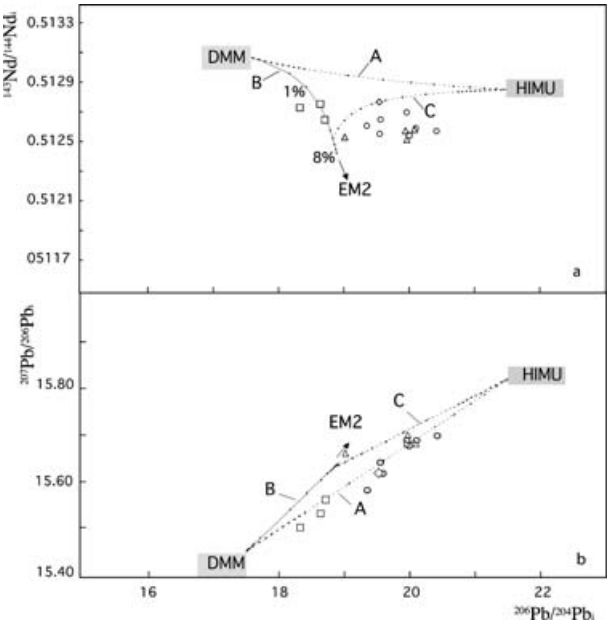

Figure 10. (a) $^{143}Nd/^{144}Nd$ v. $^{206}Pb/^{204}Pb$ and (b) $^{207}Pb/^{206}Pb$ v. $^{206}Pb/^{204}Pb$ variation diagrams for the Mamonia Upper Triassic volcanic rocks. Data source of DMM, EM2 and HIMU fields are from Zindler & Hart (1986). A = mixing line between DMM and HIMU. B = mixing line between the DMM component and a small percentage of EM2 (~ 6 %). C = mixing line between HIMU and a mantle source enriched by a small percentage of EM2.

trachytic sample CY01-24 appears to be derived from a mixing between an enriched mantle and the HIMU component. The Pb isotopic composition of this enriched mantle source could be similar to a depleted mantle source contaminated by a small percentage of an Enriched Mantle 2 component.

The $(^{143}Nd/^{144}Nd)_i$ ratios of the Mamonia volcanic (Type 1) rocks are too low to be explained by a simple mixing line between DMM and HIMU components (see mixing line A in Fig. 10a). The Pb and Nd depleted tholeiite compositions can be modelled by the mixing of a DMM mantle source with a small percentage (< 8 %) of an EM2 component without contribution of the HIMU component. The variations of the $^{143}Nd/^{144}Nd$ and $^{206}Pb/^{204}Pb$ compositions of the remaining samples (Type 2, 3 and 4) can be explained by the mixing between the enriched component of the depleted tholeiites (a small percentage of EM2) and the HIMU component (mixing line C). The trachytic sample CY01-43, characterized by the lowest $^{206}Pb/^{204}Pb$ ratio (Table 2), shows isotopic compositions which could potentially correspond to those of the component of the mixing line C (a depleted mantle source contaminated by less than 6 % of an EM2 component).

Thus, we can assume that three major components contributed to the genesis of the Mamonia suite: (1) a depleted mantle source, (2) recycled continental crust (< 5 %) and (3) an HIMU enriched source.

5.c. Temporal evolution of the Mamonia volcanism

The Upper Triassic Mamonia volcanic rocks represent the remnants of a rifted volcanic passive margin or within-plate oceanic volcanoes, located north of the African–Arabian rifted margin. They likely belong to an intra-oceanic setting because (1) they are associated with radiolarian cherts or pelagic to reefal limestones deposited in the basin, (2) no volcanic rocks are interbedded (with the exception of few alkaline dykes) within the sediments (sandstones with fossil plant remains and Halobia-bearing limestones of the Mamonia Formation or Ayios Photios Group, Fig. 3) deposited on the rifted northern African margin, and (3) the incompatible trace element ratios do not show the presence of any continental crust contamination (with the exception of recycled continental derived sediments).

The nature of the sediments, associated with the volcanic rocks, allows us to constrain the environment and depth of the volcanic eruptions. Moreover, in the Mamonia Complex, in spite of the tectonic disturbances, an evolution with time can be observed based on the petrology and chemistry of the volcanic rocks and their associated sediments. Figure 11 illustrates this evolution. Cr-spinel- and olivine-bearing basalts occur as pillowed flows interbedded with radiolarian and manganiferous cherts, and their trace element chemistry is similar to that of MORB or depleted tholeiites. These features suggest that these rocks represent the most primitive lavas of the Mamonia Complex and were generated by high degrees of partial melting. They likely represent the deepest levels of the submerged intra-oceanic shield volcanoes. With time, the sedimentary environment evolved and pelagic carbonate sediments were deposited either as interpillow voids and/or interbedded with the radiolarian cherts. Concomitantly, volcanism changed from depleted tholeiites to porphyritic alkali basalts, through oceanic island tholeiitic and mildly alkaline intersertal basalts. This evolution in magma chemistry can be attributed to a decrease of the degree of partial melting of an OIB plume and crystal fractionation in shallow magma reservoirs. During the last stages of intra-plate volcanism, shield volcanoes grew and the shallow emplacement of alkali basalts and trachytes was followed by the development of coral reefs.

5.d. Comparison of the Late Triassic Mamonia volcanism with that exposed in the Tethyan belt

Late Triassic volcanism is widely exposed in the Tethyan belt from Albania to the Indus Tsang Po suture zone of the Himalayan Ranges (Fig. 1). In SW Turkey (Antalya, Fig. 1), the Late Triassic volcanic suite consists of pillowed basaltic flows and hyaloclastites interbedded with Halobia-bearing pelagic limestones and red radiolarian cherts. They form an allochthonous unit (the Kara Dere Sayrun unit of the Middle Antalya

https://doi.org/10.1017/S0016756806002937 Published online by Cambridge University Press

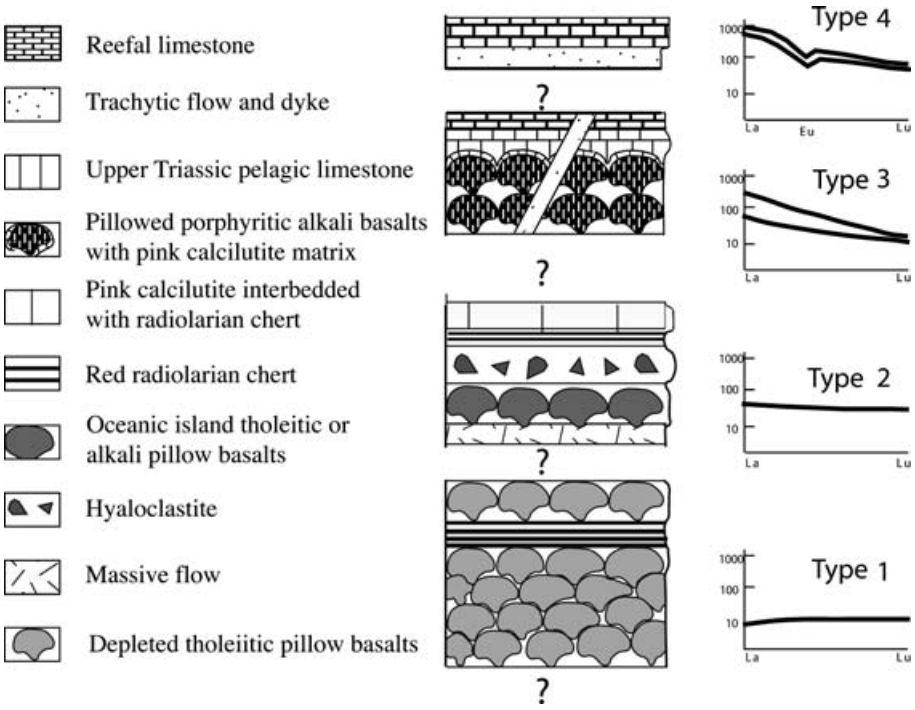

Figure 11. Reconstruction of the lithostratigraphic succession of the Mamonia Complex, showing the evolution with time of the Late Triassic volcanism and associated sedimentation. For explanation of type graphs see Figure 6.

Nappes), tectonically sandwiched between the Late Cretaceous limestones and Tertiary sediments deposited on the Arabian platform and the Late Cretaceous ophiolitic rocks (mantle rocks and ultramafic to mafic cumulates) (J. Marcoux, unpub. thesis, Univ. Paris VI, 1987). The Late Triassic sedimentary sequence (sandstones with fossil plant remains, Halobia limestones and red radiolarian cherts) is strongly similar to that exposed in the Mamonia Complex. The alkaline affinity of the Late Triassic volcanic rocks from SW Turkey has been first shown by Juteau (1975) on the basis of preserved igneous mineralogy and major element chemistry. New geochemical data (Maury *et al.* unpub. data) show that they display OIB affinities.

In northern Syria (Fig. 1), the Late Triassic volcanic and sedimentary rocks occur as blocks, broken formations and disrupted sheets within the Baër-Bassit Mélange (Al-Riyami & Robertson, 2002), which is sandwiched between the Arabian continental margin and the ophiolitic nappes. The Late Triassic volcanic rocks consist of basaltic pillow lavas and rare hyaloclastites interbedded with Halobia-bearing hemipelagic limestone, ribbon radiolarite, turbiditic calcarenite and/or massive pink micritic limestone. All these sediments were dated as Late Triassic in age by Delaune-Mayère (1984). The Late Triassic volcanic rocks contain large phenocrysts of kaersutitic hornblende, sericitized plagioclase and titaniferous augite set in a glassy groundmass now altered to zeolite, chlorite and epidote (Al-Riyami & Robertson, 2002). An alkaline affinity is shown by their major and trace element chemistry (Al-Riyami & Robertson, 2002).

In Oman, Late Triassic volcanic rocks are widespread in the Hawasina Nappes complex. The Hawasina Nappes are thrust on the Arabian platform and support the ophiolitic Semail nappe (Glennie *et al.* 1974; Béchennec *et al.* 1989, 1991; Blendinger, Van Vliet & Hughes Clarke, 1990; Pillevuit *et al.* 1997). New isotopic data (Chauvet *et al.* unpub. data) show that they present OIB affinities.

In Ladakh (Himalayan ranges), Late Triassic volcanic rocks are exposed along the Indus Tsang Po suture zone, and below the Late Jurassic Spontang and Nidar ophiolites. They belong to distinct thrust sheets (Photang sheet or Drakkar Po mélange) consisting of tectonic mélanges and distinct volcanic suites associated with oceanic sediments (Colchen, Mascle & Van Haver, 1986; Reuber, Colchen & Mevel, 1987; Corfield, Searle & Green, 1999). The Late Triassic section consists of clinopyroxene-phyric basaltic massive and pillowed flows interbedded with Halstatt facies limestone also commonly found along the interstices of pillow lavas. The Late Triassic volcanic rocks are classified as alkali basalts by Reuber, Colchen & Mevel (1987) and Corfield, Searle & Green (1999). New isotopic data (Chauvet *et al.* unpub. data) show that their εNd ratios ($5 < MgO\ wt\ \% < 6$; $2 < TiO_2\ wt\ \% < 3$) range between +4.3 and +5.3 and fall in the range of the Mamonia and Antalya nappe suites. Their trace element chemistry is similar to that of the intersertal basalts (Type 3) from SW Cyprus, but differs from that of SW Turkey by lower incompatible trace element contents (Maury *et al.* unpub. data).

https://doi.org/10.1017/S0016756806002937 Published online by Cambridge University Press

In the Himalayan and Oman ranges, rifting occurred earlier than in the eastern Mediterranean. During Permian times, (1) the Neotethyan opening was preceded by the emplacement of pre-rift continental flood basalt (Panjal traps in the Himalayan area: Bassoullet *et al.* 1980*a*; Honegger *et al.* 1982; Vannay & Spring, 1993) and (2) syn-rift tholeiitic and alkaline volcanic rocks erupted on the rifted Arabian platform while alkaline (high Ti) and tholeiitic (low Ti) melts were emplaced in the oceanic basin, floored by oceanic or transitional crust (Béchennec *et al.* 1989, 1991; Maury *et al.* 2003; Lapierre *et al.* 2004). In the Himalayan ranges, remnants of a Late Permian volcanism are tectonically imbricated with the Late Triassic alkaline basalts and interbedded with platform limestones; they consist of alkaline phonolites, the Nd composition of which suggests that they derived from an enriched mantle source without crustal contamination (Chauvet *et al.* unpub. data).

In short, the Late Triassic volcanism exhibits features of within-plate magmas (high contents in incompatible elements, Nd and Pb isotopic ratios that fall in the range of OIB) with no evidence of contamination by the continental crust all along the western Tethyan belt (Antalya to Indus). In the eastern Mediterranean, alkali basalts and hawaiites are present everywhere (Turkey, Syria, Cyprus) while trachytes and tholeiites are found solely in SW Cyprus. No evidence of initial continental rifting of the Arabian passive margin is preserved, either in the Mamonia Complex, or in the Antalya Nappes or Baër-Bassit Mélange. The oldest known units are tholeiitic and alkaline volcanic rocks and related pelagic sediments (radiolarian cherts and Halobia limestones), together with redeposited carbonates of shallow-water derivation and reefal limestones. The inferred setting for the Triassic volcanism of eastern Mediterranean is an oceanic basin, located north of the Arabian–African plate. Tectonic slices of the Mamonia Formation (Fig. 3) and dismembered units of the Baër-Bassit Mélange, and possibly the Middle Antalya nappe, can be restored as a continuous Late Triassic–Late Cretaceous deep-water succession consistent with this Triassic ocean basin interpretation.

5.e. Geodynamic implications: Late Triassic Mamonia within-plate volcanism and the Neotethys opening

Malpas, Calon & Squires (1993) suggested that part of the Mamonia Upper Triassic tholeiitic basalts (N-MORB affinities) could represent remnants of an oceanic crust. However, our results show that the Mamonia basalts which are the closest to N-MORB type on the basis of Nd and Pb isotope compositions were derived in fact from the partial melting of an enriched OIB-type mantle source. Therefore, the Late Triassic Mamonia volcanic suite is linked to the activity of a hot spot perhaps not located near an oceanic ridge. Le Roex *et al.* (1983, 1985) showed that the influence of Bouvet plume has been registered by the oceanic basalts as far as 1200 km from the hot spot. Therefore, we cannot exclude the presence of an oceanic realm during the Late Triassic (Robertson, 2000). According to our data, none of the Mamonia volcanic rocks experienced contamination by the continental crust (no Nb and Ta negative anomalies, positive εNd values), a feature consistent with their emplacement within an oceanic domain.

A question remains: is the Late Triassic volcanism of the eastern Mediterranean linked to the opening of the main Neotethyan Ocean or to that of small southerly neighbouring basins? According to most plate tectonic reconstructions (Stampfli, Marcoux & Baud, 1991; Robertson, 2000; Stampfli *et al.* 2001), the Late Triassic igneous event is linked to the break-up of the northern Gondwana margin and the opening of small ocean basins, located south of the Neotethyan realm and separated from the main ocean by rifted continental fragments where platform carbonates were deposited. The Kyrenia Range in northern Cyprus and the Bey Daglari in southern Turkey (Robertson & Woodcock, 1980) may represent such fragments. Thus, the Late Triassic Mamonia within-plate volcanism likely erupted in a small southerly Neotethyan basin floored by oceanic crust (Robertson, 2000), located south of the Kyrenia platform and north of the Eratosthenes seamount (Krashneninnikov *et al*. 1994; Kempler, 1998). The Late Triassic sediments of the Mamonia Formation (Ayios Photios Group, Fig. 3) could represent the remnants of the northern passive rifted margin of a continental micro-plate (Malpas, Calon & Squires, 1993; Robertson, 2000) rifted from the Gondwana margin. The Petra tou Romiou volcanic rocks (Dhiarrizos Group, Fig. 3) likely represent the remnants of oceanic islands, formed outboard of the continental micro-plate, currently represented by the Eratosthenes seamount.

Another question concerns the structural evolution of the Mamonia Complex. Everywhere in the Tethyan belt, the Triassic volcanic rocks are thrust by the ophiolitic nappes and themselves thrust upon the Gondwanian platform. The only exception seems to be Cyprus and some local sections in Baër-Bassit, where out-of-sequence thrusting occurred (Al-Ryami & Robertson, 2002).

In our opinion, as Cyprus suffered several tectonic events (Grand *et al.* 1993; Bailey, Holdsworth & Swarbrick, 2000), out-of-sequence thrusting affected Cyprus in the same way as Baër-Bassit. This is demonstrated by the section of Ayia Varvara (Fig. 2b), where we observe the superposition of lavas of the Mamonia Complex, below a sheet of amphibolite, and below a sheet of peridotite. This kind of superposition (ophiolite–metamorphic sole–Triassic lavas), observed everywhere in the Tethyan belt, is the result of the oldest tectonic event. In Cyprus the original tectonic pile was

https://doi.org/10.1017/S0016756806002937 Published online by Cambridge University Press

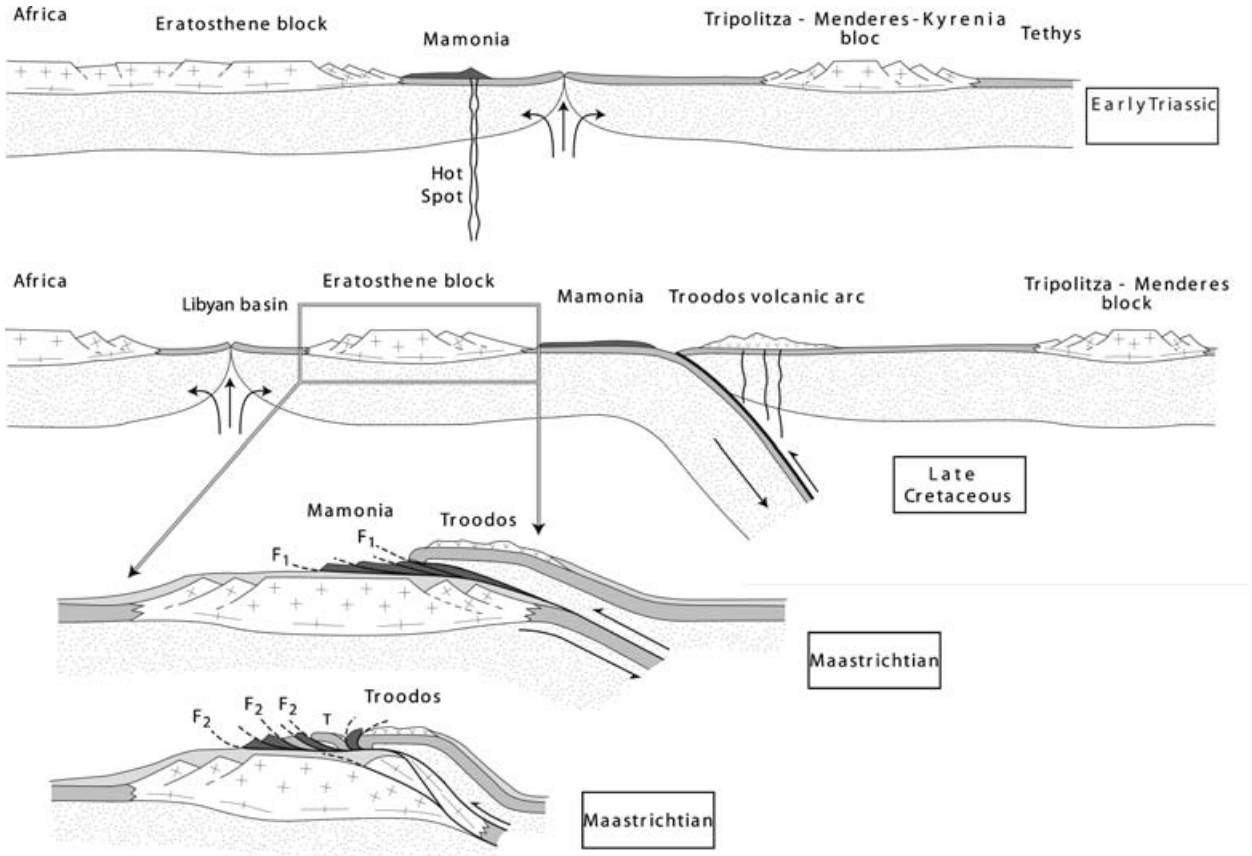

Figure 12. Schematic reconstruction of the structural pattern of the Troodos and Mamonia complexes involving two tectonic events of Late Cretaceous age.

later more or less modified by superposed younger tectonic events.

6. Conclusions

Our results show that the Mamonia Complex (SW Cyprus) represents remnants of Late Triassic intra-oceanic within-plate volcanism, which evolved with time. Volcanic activity started with the eruption of depleted olivine tholeiites (Type 1) associated with deep basin siliceous and/or calcareous sediments, accompanied and/or followed by oceanic island tholeiites (Type 2). With time, volcanism evolved towards highly phyric alkali basalts (Type 3) enriched in the most incompatible elements (Nb, Ta, Th) and LREE, interbedded with pelagic Halobia-bearing limestones or reef limestones. Highly LREE-enriched trachytes (Type 4) characterize the end of volcanic activity. The trace element features of the four rock types are likely linked to different partial melting ratios of heterogeneous OIB sources. Nd and Pb isotope ratios suggest that the mildly alkali basalts derived from heterogeneous enriched mantle sources. The trachytes cannot be derived by fractional crystallization of the alkali basalts but more likely from partial melting at depth of mafic material that shares with the alkali basalts similar trace element and isotopic compositions.

Late Triassic volcanism similar to that of the Mamonia Complex can be traced from the Himalayas to the Eastern Mediterranean (southern Taurides, Baër-Bassit) through Oman, and was likely located offshore with respect to the southern Neotethyan passive margin. Finally, Nd and Pb isotope compositions of the depleted olivine tholeiites show that these rocks cannot represent remnants of a Late Triassic normal oceanic crust.

The present day structural pattern of the Mamonia Complex and Troodos–Akamas ophiolites is probably due to two compressional events. The older one (F1, Fig. 12), related to the obduction of the ophiolites and the overthrust of deep-basin sedimentary and volcanic rocks upon the Neotethyan margin, took place during Maastrichtian time. The younger one (F2, Fig. 12) was related to the tectonic imbrication of the Mamonia and Troodos complexes which also occurred during the Maastrichtian with a vergence similar to that of the first event.

Acknowledgements. This work was funded by the teams UMR 5025 of the Centre National de la Recherche Scientifique, Université Joseph Fourier (Grenoble) and Université de Savoie. We thank Dr L. A. Coogan and anonymous reviewers for their helpful comments to improve the manuscript. This paper is dedicated to the memory of our friend Henriette Lapierre, first author of this manuscript, who died suddenly on 14 January 2006 during a field excursion in Syria.

Henriette started her scientific career working on the geology of Cyprus 40 years ago during her Ph.D. and prematurely ended it with the present work.

References

ABOUCHAMI, W., GALER, S. J. G. & HOFMANN, A. W. 2000. High precision lead isotope systematics of lavas from the Hawaiian Scientific Drilling Project. *Chemical Geology* **169**, 187–209.

ALLÈGRE, C. J., LEWIN, E. & DUPRÉ, B. 1988. A Coherent Crust Mantle Model for the Uranium Thorium Lead Isotopic System. *Chemical Geology* **70**, 211–34.

AL-RIYAMI, K., ROBERTSON, A. H. F., XENOPHONTOS, C., DANELIAN, T. & DIXON, J. E. 2000. Tectonic evolution of the Mesozoic Arabian passive continental margin and related ophiolite in Baër-Bassit region (NW Syria). In *Proceedings of the Third International Conference on the Geology of the Eastern Mediterranean, Nicosia* (eds I. Panayides, C. Xenophontos and J. Malpas), pp. 61–81. Cyprus Geological Survey.

AL-RIYAMI, K. & ROBERTSON, A. H. F. 2002. Mesozoic sedimentary and magmatic evolution of the Arabian continental margin, northern Syria: Evidence from the Baër-Bassit Melange. *Geological Magazine* **139**, 395–420.

BAILEY, W. R., HOLDSWORTH, R. E. & SWARBRICK, R. E. 2000. Kinematic history of a reactivated oceanic suture: the Mamonia Complex Suture Zone, SW Cyprus. *Journal of the Geological Society, London* **157**, 1107–26.

BARRAT, J. A., KELLER, F. & AMOSSÉ, J. 1996. Determination of rare earth elements in sixteen silicate reference samples by ICP-MS after Tm addition and ion exchange separation. *Geostandards Newsletter* **20**, 133–9.

BASSOULLET, J. P., BOULIN, J., COLCHEN, M., MARCOUX, J., MASCLE, G. & MONTENAT, C. 1980*a*. Evolution des domaines téthysiens du pourtour du bouclier indien du Carbonifère au Crétacé. Géologie des chaînes alpines issues de la Téthys. Colloque C5, 26ème Congrès Géologique International, Paris. *Mémoires du Bureau de Recherches Géologiques et Minières* **115**, 180–98.

BASSOULLET, J. P., COLCHEN, M., JUTEAU, T., MARCOUX, J. & MASCLE, G. 1980b. L'édifice des nappes de Zanskar (Ladakh, Himalaya). *Comptes Rendus de l'Académie des Sciences, Paris* **290**, 389–92.

BÉCHENNEC, F., LE MÉTOUR, J., RABU, D., BEURRIER, M., BOURDILLON-JEUDY-DE-GRISSAC, C., DE WEVER, P., TEGYEY, M. & VILLEY, M. 1989. Géologie d'une chaîne issue de la Téthys: les montagnes d'Oman. *Bulletin de la Société géologique de France* (s. 8) **t. V**(2), 231–40.

BÉCHENNEC, F., TEGYEY, M., LE MÉTOUR, J., LEMIÈRE, B., LESCUYER, J.-L., RABU, D. & MILÉSI, J.-P. 1991. Igneous rocks in the Hawasina nappes and the Hajar supergroup, Oman mountains: their significance in the birth and evolution of the composite extensional margin of Eastern Tethys. In *Ophiolite genesis and evolution of the oceanic lithosphere* (ed. Director at General of Minerals), pp. 569–611. Ministry of Petroleum and Minerals, Oman.

BLENDINGER, W., VAN VLIET, A. & HUGHES CLARKE, M. W. 1990. Updoming, rifting and continental margin development during the Late Paleozoic in Northern Oman. In *The geology and tectonics of the Oman region* (eds A. H. F. Robertson, M. P. Searle and A. C. Ries), pp. 27–37. Geological Society of London, Special Publication no. 49.

BRAGIN, N. Y., BRAGINA, L. G. & KRYLOV, K. A. 2000. Albian–Cenomanian deposits of the Mamonia Complex, southwestern Cyprus. In *Proceedings of the Third International Conference on the Geology of the Eastern Mediterranean, Nicosia* (eds I. Panayides, C. Xenophontos and J. Malpas), pp. 309–17. Cyprus Geological Survey.

CANNAT, M. & MASCLE, G. 1990. Réunion extraordinaire de la Société Géologique de France en Himalaya du Ladakh. *Bulletin de la Société géologique de France* (s. 8) **t. VI**(4), 553–82.

CLUBE, T. M. & ROBERTSON, A. H. F. 1986. The paleorotation of the Troodos ophiolite, Cyprus, in the Late Mesozoic–Early Cenozoic plate tectonic framework of the Eastern Mediterranean. *Surveys in Geophysics* **8**, 239–55.

COLCHEN, M., MASCLE, G. & VANHAVER, TH. 1986. Some aspects of the collision tectonics in the Indus suture zone, Ladakh Himalaya. In *Collision Tectonics* (eds M. P. Coward and A. C. Ries), pp. 173–84. Geological Society of London, Special Publication no. 19.

CORFIELD, R. I., SEARLE, M. P. & GREEN, O. R. 1999. Photang thrust sheet: An accretionary complex structurally below the Spontang ophiolite constraining timing and tectonic environment of ophiolite obduction, Ladakh Himalaya, NW India. *Journal of the Geological Society, London* **156**, 1031–44.

DELAUNE-MAYÈRE, M. 1984. Evolution of a Mesozoic passive continental margin: Baer-Bassit (NW Syria). In *The geological evolution of the Eastern Mediterranean* (eds D. J. Dixon and A. H. F. Robertson), pp. 151–75. Geological Society of London, Special Publication no. 17.

DELAUNE-MAYÈRE, M. & PARROT, J.-F. 1976. Evolution du Mésozoïque de la marge continentale méridionale du bassin téthysien oriental d'après les études des séries sédimentaires de la région ophiolitique du NW syrien. *Cahiers ORSTOM, Série Géologie* **8**(2), 173–84.

DUMONT, J.-F., GUTNIC, M., Z, J. & POISSON, A. 1972. Le Trias des Taurides occidentales (Turquie). Définition du bassin Pamphylien: un nouveau domaine à ophiolites à la marge externe de la chaîne taurique. *Zeitschrift der Deutschen Geologischen Gesellschaft* **123**, 385–409.

EALEY, P. J. & KNOX, G. J. 1975. The pre-Tertiary rocks of S.W. Cyprus. *Geologie en Mijnbouw* **54**, 85–100.

GASS, I. G. 1980. The Troodos massif: Its role in the unravelling of the ophiolite problem and its significance in the understanding of constructive plate margin processes. In *Ophiolites* (ed. A. Panayiotou), pp. 21–3. Proceedings International Ophiolite Symposium Cyprus, Nicosia.

GLENNIE, K. W., BOEUF, M. G., HUGHES CLARKE, M. W., MOODY-STUART, M., PILAAR, W. F. & REINHART, B. M. 1974. *Geology of the Oman Mountains*. Verhandelingen van het Koninklijk Nederlands geologisch minjbouwkundig Genootschap [Transactions of the Royal Dutch Geological and Mining Society] vol. **31**, part 1, 423 pp.

GRAND, T., LAPIERRE, H., MASCLE, G., OHNENSTETTER, M. & ANGELIER, J. 1993. Superimposed tectonics of the Cyprus ophiolitic massifs. *Tectonics* **12**, 93–101.

HONEGGER, K., DIETRICH, V., GANSSER, A., HOENI, M. & TROMMSDORFF, V. 1982. Magmatism and metamorphism in the Ladakh Himalayas (the Indus-Tsangpo suture zone). *Earth and Planetary Science Letters* **60**, 253–92.

JUTEAU, T. 1975. *Les ophiolites des nappes d'Antalya (Taurides occidentales, Turquie): pétrologie d'un fragment de*

https://doi.org/10.1017/S0016756806002937 Published online by Cambridge University Press

l'ancienne croûte océanique téthysienne? Science de la Terre Mémoire no. 5. Nancy, France, 692 pp.

KEMPLER, D. 1998. Eratosthenes Seamount: the possible spearhead of incipient continental collision in the Easternmost Mediterranean. In *Proceedings of the Ocean Drilling Program, Scientific Results, vol 160* (eds A. H. F. Robertson, K.-C. Emeis, C. Richter and A. Camerlenghi), pp. 68–71. College Station, Texas.

KIEFFER, B., ARNDT, N. T. & WEISS, D. 2002. Petrology and geochemistry of a bimodal alkalic shield volcano, Site 1139, Kerguelen Plateau. *Journal of Petrology* **43**, 1259–86.

KRASHENINNIKOV, V. A., UDINTSEV, G. B., MOURAVIOV, V. & HALL, J. K. 1994. Geological structure of the Eratosthenes Seamount. In *Geological structure of the North-Eastern Mediterranean* (Cruise 5 of the Research Vessel Akademik Nikolaj Strakhov) (eds V. A. Krasheninnikov and J. K. Hall), pp. 113–30. Jerusalem, Israel: Historical Productions-Hall, Ltd.

LAPIERRE, H. 1968. Découverte d'une série volcano-sédimentaire probablement d'âge Crétacé supérieur au S-W de l'île de Chypre. *Comptes Rendus de l'Académie des Sciences, Paris* **266**, 1817–20.

LAPIERRE, H. 1975. *Les formations sédimentaires et éruptives des nappes de Mamonia et leurs relations avec le Massif du Troodos (Chypre occidentale).* Mémoires de la Société géologique de France no. 123, 127 pp.

LAPIERRE, H. & PARROT, J.-F. 1972. Identité géologique des régions de Paphos (Chypre) et de Baër-Bassit (Syrie). *Comptes Rendus de l'Académie des Sciences, Paris* **274**, 1999–2002.

LAPIERRE, H. & ROCCI, G. M. 1970. Un bel exemple d'association cogénétique laves-radiolarites-calcaires: la formation triasique de Pétra tou Romiou (Chypre). *Comptes Rendus de l'Académie des Sciences, Paris* **268**, 2637–40.

LAPIERRE, H. & ROCCI, G. M. 1976. Le volcanisme alcalin du Sud-Ouest de Chypre et le problème de l'ouverture des régions téthysiennes au Trias. *Tectonophysics* **30**, 299–313.

LAPIERRE, H., DUPUIS, V., MERCIER DELÉPINAY, B., TARDY, M., RUIZ, J., MAURY, R. C., HERNANDEZ, J. & LOUBET, M. 1997. Is the Lower Duarte Igneous Complex (Hispaniola) a remnant of the Caribbean plume generated oceanic plateau? *Journal of Geology* **105**, 111–20.

LAPIERRE, H., SAMPER, A., BOSCH, D., MAURY, R. C., BÉCHENNEC, F., COTTEN, J., DEMANT, A., BRUNET, A., KELLER, F. & MARCOUX, J. 2004. The Tethyan plume: Geochemical diversity of Middle Permian basalts from the Oman rifted margin. *Lithos* **74**, 167–98.

LEGENDRE, C., MAURY, R. C., SAVANIER, D., COTTEN, J., CHAUVEL, C., HÉMOND, C., BOLLINGER, C., GUILLE, G., BLAIS, S. & ROSSI, P. 2005. The origin of intermediate and evolved lavas in the Marquesas archipelago: an example from Nuku Hiva island (French Polynesia). *Journal of Volcanology and Geothermal Research* **143**, 293–317.

LE ROEX, A. P., DICK, H. J. B., ERLANK, A. J., REID, A. M., FREY, F. A. & HART, S. R. 1983. Geochemistry, mineralogy and petrogenesis of lavas erupted along the southwest Indian Ridge between the Bouvet Triple Junction and 11 Degrees East. *Journal of Petrology* **24**, 267–318.

LE ROEX, A. P, DICK, H. J. B., REID, A. M., FREY, F. A., ERLANK, A. J. & HART, S. R. 1985. Petrology and geochemistry from the American–Antarctic Ridge, Southern Ocean: implications for the westward influence of the Bouvet mantle plume. *Contributions to Mineralogy and Petrology* **90**, 367–80.

MAHÉO, G., BERTRAND, H., GUILLOT, S., MASCLE, G., PÊCHER, A., PICARD, C. & DESIGOYER, J. 2000. Les ophiolites crétacées du Sud Ladakh (NW Himalaya, Inde): Témoins d'un arc immature intra-océanique. *Comptes Rendus de l'Académie des Sciences, Paris* **300**, 289–95.

MALPAS, J., CALON, T. & SQUIRES, G. 1993. The development of a Late Cretaceous microplate suture zone in SW Cyprus. In *Magmatic Processes and Plate Tectonics* (eds H. Prichard, T. Alabaster, N. B. Harris and C. R. Neary), pp. 177–95. Geological Society of London, Special Publication no. 76.

MALPAS, J., XENOPHONTOS, C. & WILLIAMS, D. 1992. The Ayia Varvara Formation of SW Cyprus, a product of collisional tectonics. *Tectonophysics* **212**, 193–211.

MARCOUX, J. 1970. Age carnien des termes effusifs du cortège ophiolitique des Nappes d'Antalya (Taurus Lycien –oriental, Turquie). *Comptes Rendus de l'Académie des Sciences, Paris* **271**, 227–41.

MAURY, R. C., BÉCHENNEC, F., COTTEN, J., CAROFF, M., CORDEY, F. & MARCOUX, J. 2003. Late Permian plume-related magmatism of the Hawasina Nappes and the Arabian Platform: Incidences on the evolution of the Neotethyan margin in Oman. *Tectonics* **22**(6), 1073, doi:10.1029/2002TC001483.

MCCULLOCH, M. T. & WASSERBURG, G. J. 1978. Sm–Nd and Rb–Sr chronology of continental crust formation. *Science* **200**, 1003–11.

MCLEOD, C. J. 1990. Role of the Southern Troodos Transform Fault in the rotation of the Cyprus microplate: Evidence from the Eastern Limassol Forest Complex. In *Ophiolites. Oceanic Crustal Analogues* (eds J. Malpas, E. Moores, A. Panayiotou and C. Xenophontos), pp. 75–86. Proceedings of 'Troodos 87' Symposium. Cyprus Geological Survey.

MCLEOD, C. J. & MURTON, B. J. 1995. On the sense of the slip of the Southern Troodos transform fault zone. *Geology* **23**, 257–60.

MURTON, B. J. 1990. Was the Southern Troodos Transform Fault a victim of microplate rotation? In *Ophiolites. Oceanic Crustal Analogues* (eds J. Malpas, E. Moores, A. Panayiotou and C. Xenophontos), pp. 87–98. Proceedings of 'Troodos 87' Symposium. Cyprus Geological Survey.

PARROT, J.-F. 1974a. Les différentes manifestations effusives de la région ophiolitique du Baër-Bassit (N-W de la Syrie), Comparaison pétrographique et géochimique. *Comptes Rendus de l'Académie des Sciences, Paris* **279**, 627–30.

PARROT, J.-F. 1974b. L'assemblage ophiolitique du Baër-Bassit (N-W de la Syrie): étude pétrographique et géochimique du complexe filonien, des laves qui lui sont associées et d'une partie des formations effusives comprises dans le volcano-sédimentaire. *Cahiers ORSTOM, Série Géologie* **6**(2), 97–126.

PILLEVUIT, A., MARCOUX, J., STAMPFLI, G. & BAUD, A. 1997. The Oman Exotics: a key to the understanding of the Neotethyan geodynamic evolution. *Geodinamica Acta* **10**, 209–38.

REUBER, I., COLCHEN, M. & MEVEL, C. 1987. The geodynamic evolution of the South-Tethyan margin in Zanskar, NW-Himalaya, as revealed by the Spongtang ophiolitic melanges. *Geodinamica Acta* **1**, 283–96.

ROBERTSON, A. H. F. 1977. The Kannaviou, Cyprus: volcaniclastic sedimentation of a probable Late Cretaceous volcanic arc. *Journal of the Geological Society, London* **133**, 447–66.

ROBERTSON, A. H. F. 2000. Tectonic evolution of Cyprus in its easternmost Mediterranean setting. In *Proceedings of the Third International Conference on the Geology of the eastern Mediterranean, Nicosia* (eds I. Panayides, C. Xenophontos and J. Malpas), pp. 11–44. Cyprus Geological Survey.

ROBERTSON, A. H. F. & WALDRON, J. W. 1990. Geochemistry and tectonic setting of Late Triassic and Late Jurassic–Early Cretaceous basaltic extrusives from the Antalya Complex, south west Turkey, In *Proceedings of the International Earth Sciences Congress on Aegean Region* (eds M. Y. Savasçin and A. H. Eronat), pp. 279–99. IESCA Publication no. 2, Izmir, Turkey.

ROBERTSON, A. H. F. & WOODCOCK, N. H. 1980. Tectonic setting of the Troodos in the East Mediterranean. In *Ophiolites; Proceedings, International Ophiolite Symposium, Nicosia* (ed. A. Panayiotou), pp. 36–49. Cyprus Geological Survey.

ROBERTSON, A. H. F. & WOODCOCK, N. H. 1982. Sedimentary history of the segment of the Mesozoic–Tertiary Antalya continental margin, Turkey. *Eclogae Geologicae Helvetiae* **75**, 517–62.

ROCCI, G. M., BAROZ, F., Bébien, J., DESMET, A., LAPIERRE, H., OHNENSTETTER, D., OHNENSTETTER, M. & PARROT, J.-F. 1980. The Mediterranean ophiolites and their related Mesozoic volcano-sedimentary sequences. In *Ophiolites; Proceedings, International Ophiolite Symposium, Nicosia* (ed. A. Panayiotou), pp. 273–86. Cyprus Geological Survey.

SEARLE, M. P. 1983. Stratigraphy, structure and evolution of the Tibetan–Tethys zone in Zanskar and the Indus suture zone in the Ladakh Himalaya. *Transactions of the Royal Society of Edinburgh, Earth Sciences* **73**, 205–19.

SHERVAIS, J. W. 1982. Ti–V plots and the petrogenesis of modern and ophiolitic lavas. *Earth and Planetary Science Letters* **59**, 101–18.

STAMPFLI, G. M., MARCOUX, J. & BAUD, A. 1991. Tethyan margin in space and time. *Palaeogeography, Palaeoclimatology, Palaeoecology* **87**, 373–409.

STAMPFLI, G. M., BOREL, G., CAVAZZA, W., MOSAR, J. & ZIEGLER, P. A. 2001. *The Paleotectonic Atlas of the Peri-Tethyan Domain (CD-ROM)*. European Geophysical Society.

SUN, S. S. & MCDONOUGH, W. F. 1989. Chemical and isotopic systematics of ocean basalts: Implications for the mantle composition and processes. In *Magmatism in the ocean basins* (eds A. D. Saunders and M. J. Norry), pp. 313–45. Geological Society of London, Special Publication no. 42.

SWARBRICK, R. E. 1993. Sinistral strike-slip and transpressional tectonic in an ancient ocean setting: The Mamonia complex, southwest Cyprus. *Journal of the Geological Society, London* **150**, 381–92.

SWARBRICK, R. E. & NAYLOR, M. A. 1980. The Kathikas Melange, southwest Cyprus: Late Cretaceous, submarine debris flows. *Sedimentology* **27**, 63–78.

SWARBRICK, R. E. & ROBERTSON, A. H. F. 1980. Revised stratigraphy of the Mesozoic rocks of southern Cyprus. *Geological Magazine* **117**, 547–63.

TODT, W., CLIFF, R. A., HANSER, A. & HOFMANN, A. W. 1996. Evaluation of a 202Pb–205Pb double spike for high-precision lead isotope analysis. In *Earth processes: Reading the isotopic code* (eds A. Basu and S. Hart), pp. 429–37. American Geophysical Union, Geophysical Monograph no. 95.

VANNAY, J. C. & SPRING, L. 1993. Geochemistry of the continental basalts within the Tethyan Himalaya of Lahul-Spiti and SE Zanskar, NW India. In *Himalayan Tectonics* (eds P. J. Treloar and M. P. Searle), pp. 237–49. Geological Society of London, Special Publication no. 74.

WHITE, M. W., ALBARÈDE, F. & TELOUK, F. 2000. High-precision analysis of Pb isotopic ratios by multi-collector ICP-MS. *Chemical Geology* **167**, 257–70.

WINCHESTER, J. A. & FLOYD, P. A. 1977. Geochemical discrimination of different magma series and their differentiation products using immobile elements. *Chemical Geology* **20**, 325–43.

ZINDLER, A. & HART, S. R. 1986. Chemical geodynamics. *Annual Review of Earth and Planetary Sciences* **14**, 493–571.